Table 1
Concentrations of DE constituents.

	Concentrations
DE particle mass (mg/m^3)	1.0
CO (ppm)	2.67
NO_2 (ppm)	0.23
SO_2 (ppm)	<0.01

nervous system (CNS), this was not well understood in vivo. The present study was designed to investigate the impact on the CNS (e.g., motor function) in DE exposed mice using a behavioral test and measuring the levels of dopamine and its metabolites in the striatum and nucleus accumbens.

The present study was conducted in accordance with the Guiding Principles for the Care and Use of Laboratory Animals, Tokyo University of Science adopted by the Committee on Animal Research of Tokyo University of Science. All efforts were made to minimize the number of animals used and their suffering. All experiments were conducted using pregnant ICR mice obtained from SLC Co. (Shizuoka, Japan). Pregnant mice were exposed to DE for 8 h, 5 days per week (from Monday to Friday, 9:00–17:00) in an inhalation chamber (Japan Anti-Tuberculosis Association, Kiyose, Tokyo) from gestational day (GD) 2 to GD 17. After DE exposure, mothers and male pups were maintained in a clean room. Control animals were kept in a clean room. Each pup was weaned on postnatal day 21, after which male mice were transported to Tokyo University of Science. Animals were acclimated for 2 weeks and were exposed to a 12-h light/dark cycle (lights on from 8:00 to 20:00). Food and water were provided ad libitum. All experimental mice were handled in accordance with institutional and national guidance for the care and use of laboratory animals.

A 2369-cc diesel engine (Isuzu Motors, Ltd., Tokyo, Japan) was operated at a speed of 1050 rpm and 80% load, using a commercial light oil. Exhaust was introduced into a stainless steel dilution tunnel (218-mm diameter × 5.55 m). In the tunnel, the exhaust was mixed with clean air, and average concentrations of exhaust constituents were maintained at 1.0 mg/m^3 for particles, 2.67 ppm for CO, 0.23 ppm for NO_2, and less than 0.01 ppm for SO_2 (Table 1).

To investigate DE-induced behavioral changes, we used an activity monitor with an infrared ray sensor (NS-AS01; Neuroscience Inc., Tokyo, Japan) to measure spontaneous motor activity (SMA) by the release of temperature-associated infrared rays. SMA was counted at 10 min intervals for 2 days. Data were automatically analyzed with a computerized system (multidigital 32-port counter system; Neuroscience Inc.).

Following the behavioral test, mice were killed by decapitation and brains were immediately collected as samples. In the daytime, the brain was dissected into striatum and nucleus accumbens, immediately frozen in liquid nitrogen, and stored at −80 °C until neurochemical analysis.

Frozen brain tissue was homogenized in ice-cold 0.2 M perchloric acid (Nakalai Tesque, Inc., Kyoto, Japan) containing 100 μM EDTA 2Na (Dojindo Laboratories, Kumamoto, Japan) and 1 ng/mL isoproterenol as an internal standard (Sigma–Aldrich Co., St. Louis, MO). Homogenates were placed on ice for 30 min and centrifuged at 20,000 × *g* at 0 °C for 15 min. The pellets were used for protein assay. Supernatants were mixed with 1 M sodium acetate to adjust the pH to 3.0 (Kanto Chemical Co., Inc., Tokyo, Japan) and were immediately frozen in liquid nitrogen and stored at −80 °C until analysis.

10 μL of the final supernatant was injected with a microsyringe (702 SNR; Hamilton, Co., Reno, NV) into a high-performance liquid chromatography (HPLC) system equipped with an electrochemical detector (HTEC-500MAB; EICOM, Kyoto, Japan). The standard solution contained dopamine (DA; Sigma–Aldrich Co.) and its metabolites: 3,4-dihydroxyphenylacetic acid (DOPAC; Wako Pure Chemical Industries, Ltd., Osaka, Japan), and homovanillic acid (HVA; Sigma–Aldrich Co.). Separation of DA and its metabolites was performed on a C18 reverse-phase column (Eicompak SC-5ODS; Ø 3.0 mm × 150 mm; Eicom), maintained at 25 °C with an electrochemical detector (EPC-500, Eicom). The mobile phase was 0.1 M acetic acid/citric acid buffer (pH 3.5) containing EDTA 2Na (5 mg/L), octanesulfonic acid (190 mg/L; Nakalai Tesque), and methanol (15%, v/v; Kanto Chemical Co., Inc.). The flow rate was maintained at 0.5 mL/min. Data were collected and analyzed with PowerChrom version 2.3 chromatography software (eDAQ Pty, Ltd., New South Wales, Australia), with the use of area ratios to determine sample concentrations.

Pellets were resuspended in 100 mM Tris–HCl for protein determination by high-sensitivity Bradford method with a commercial reagent (ADV-01; Cytoskelton, Inc., Deriver, CO) and measurements were performed according to the manufacturer's protocol. Absorbance was read at 595 nm on a 96-well microplate reader (Model 550; BioRad, Hercules, CA) and protein concentration was calculated from a standard curve generated with the use of bovine gamma globulin (Pre-Diluted Protein Assay Standards; Bovine Gamma Globulin Set; Biotechnology, Inc., Rockford, IL).

Concentrations of DA and its metabolites are expressed as nanograms per milligram of protein, while the catabolism rate is expressed as the ratio of metabolites to DA and indicated by the index of catabolism rate (i.e., DOPAC/DA, HVA/DA, DOPAC+HVA/DA). Indices were calculated from individual tissue samples.

The results were analyzed by two-way ANOVA with replication and by unpaired *t*-test: the Mann–Whitney *U*-test was used for comparison between the two groups. All data are reported as means ± S.E.M.

There have been increasing reports that neurodegenerative disorders may begin in the early stages of development and environmental factor may be a key role [3]. In the present study, prenatal exposure to DE in male mice decreased spontaneous motor activity (Fig. 1A). According to environmental standard value in Tokyo metropolitan, suspended particles matter (SPM) concentration in the environment is 0.1 mg/m^3. DEP is included approximately 40% in SPM. Considering the duration of exposure, the DEP concentration in this study was 6-hold greater than that of environment. It has been reported that the mice exposed to DE during adult or neonatal periods showed less spontaneous locomotor activity than that of controls in standard running wheel cages [11]. The DE concentration in that study was 6 mg DEP/m^3, approximately 6-fold greater than that in the present study. Our result indicates that the lower concentration of DE could affect offspring locomotion in mice. Interestingly, we also showed that DE exposed mice exhibited decreased locomotor activity during the light phase in comparison to the control mice (Fig. 1B). This result might suggest that the regulation of the sleep-arousal cycle of maternally DE exposed mice is affected. It is well known that noradrenaline (NA) in locus ceruleus and serotonin (5-HT) in raphe nucleus activities changes with the sleep-arousal cycle [20]. Our findings suggest the possibility that prenatal exposure to DE may affect the persistent changes in the NA and the 5-HT system. On the other hand, dopaminergic mechanisms within the striatum and nucleus accumbens play an important role in the control of locomotor activity, and a change in DA turnover depends essentially on a change in impulse flow in the dopamine neurons [9]. Isoflurane, for example, has been shown to induce hyperlocomotion during emergence and may be associated with increased DA turnover in the striatum and nucleus accumbens [7]. Moreover benzo[*a*]pyrene, included in DE suppressed DA in the striatum and DA turnover in the nucleus accumbens [10]. To inves-

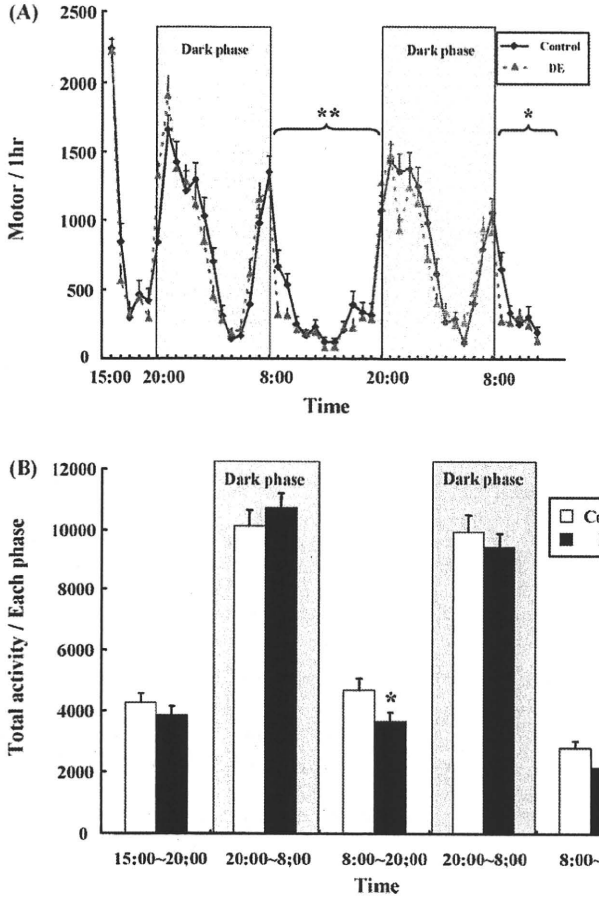

Fig. 1. Effect of prenatal exposure to diesel exhaust (DE) on spontaneous motor activity (SMA) in mice. (A) The data were expressed as time-course changes in control and DE exposed mice. The DE-exposed group revealed significant alterations of SMA. Each point represents the mean activity and counts for 1 h ± S.E.M of 27 mice. $^{*}p < 0.05$ vs. control, $^{**}p < 0.01$ vs. control. (B) The data were expressed as total SMA in control and DE exposure mice. SMA was significantly decreased in DE-exposed group compared to that in control group. Each column represents the mean total activity counts ± S.E.M of 27 mice. $^{*}p < 0.05$ vs. control group.

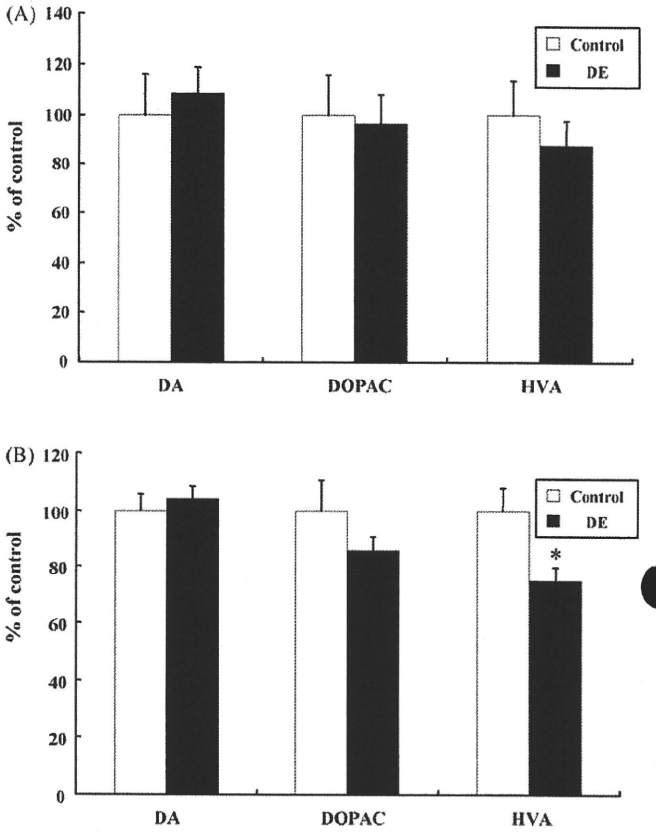

Fig. 2. Effect of prenatal exposure to diesel exhaust (DE) on dopamine (DA) and its metabolites (DOPAC, HVA). (A) Levels of DA and its metabolites in the striatum. The data were expressed as a percentage of the value in control mice. Each column represents the mean ± S.E.M of nine vs. eight mice. $^{*}p < 0.05$ vs. control group. (B) Levels of DA and its metabolites in the nucleus accumbens. The data were expressed as a percentage of the value in control mice. Each column represents the mean ± S.E.M. of nine mice. $^{*}p < 0.05$ vs. control group.

tigate the possibility that maternally inhaled DE has an effect on the dopaminergic system in vivo, we measured the levels of DA and its metabolites using HPLC in the striatum and nucleus accumbens. There were no changes in either brain region detected between the DE exposed mice and the control mice in DA levels (Fig. 2A and B, Table 2), however, HVA concentrations were decreased in DE exposed mice (Fig. 2B, Table 2). Extracellular HVA concentration was used as an index of changes in DA release [2]. These results indicate that maternal exposure to DE caused hypolocomotion via DA turnover reduction in the striatum and nucleus accumbens. HVA production depends on catechol-*O*-methyltransferase (COMT) activity. It is well accepted that this activity is widely distributed in mammalian brains [13,16]. Reduction in COMT could affect the turnover of DA, likely leading to neuron loss and motor deficits in

Table 2
Amounts of DA and its metabolites (ng/mg protein) and values of DA turnover in the striatum and nucleus accumbens.

Brain region	Group	Content (ng/mg)		
		DA	DOPAC	HVA
Striatum	Control	179.21 ± 29.06	26.59 ± 4.25	30.38 ± 4.16
	DE	194.83 ± 18.29	25.71 ± 3.08	26.62 ± 3.10
Nucleus accumbens	Control	149.33 ± 8.75	29.50 ± 3.16	27.29 ± 2.18
	DE	155.50 ± 6.74	25.32 ± 1.48	20.43 ± 1.30*
Brain region	Group	Turnover		
		DOPAC/DA	HVA/DA	(DOPAC+HVA)/DA
Striatum	Control	0.17 ± 0.03	0.22 ± 0.05	0.39 ± 0.08
	DE	0.13 ± 0.01*	0.13 ± 0.01**	0.27 ± 0.01**
Nucleus accumbens	Control	0.20 ± 0.02	0.18 ± 0.01	0.38 ± 0.03
	DE	0.16 ± 0.01	0.13 ± 0.01***	030 ± 0.01**

The data were expressed as mean ± S.E.M. $^{*}p < 0.05$ vs. control, $^{**}p < 0.01$ vs. control, $^{***}p < 0.001$ vs. control.

the striatum [25]. Taken together, our findings suggest the possibility that the prenatal exposure to DE might alter the activity of COMT in mice striatum and nucleus accumbens.

DA neurons have an ability to reduce antioxidant capacity and are more susceptible to oxidative stress, such as superoxide and hydrogen peroxide, relative to other cell types [12]. Low DEP selectively damages DA neurons through the phagocytic activation of microglial NADPH oxidase and oxidative insult in vitro [1]. Additionally, it has been reported that the substantia nigra contains many microglia in comparison to the cortex [8]. These findings indicate that dopamine neuron could be influenced by DE exposure. Furthermore, Sugamata et al. found that prenatal exposure to DE has diffuse and extensive pathological effects on the various regions of brain. Maternal exposure to DE showed evidence of numerous caspase-3-positive cells and of what appeared to be ultrafine, DEP [22]. These observations may support the idea that DEP contained in DE can enter the fetal brain and cause the cell death directly, resulting in the dysfunction of the dopaminergic system in mice.

In conclusion, we observed that the motor activity of DE-exposed mice was clearly decreased in vivo and DA turnover in the striatum and nucleus accumbens. Although we cannot exclude the possibility that prenatal exposure to DE might affect other monoaminergic systems, such as NA and 5-HT, prenatal DE exposure may affect the development of the CNS. Further investigation is needed to fully understand the mechanism how inhaled DE impaired DA neurons in the CNS.

Acknowledgments

We thank Mr. Tadashi Udagawa (Research Institute of Tuberculosis) for help with DE-exposure, and the students in Takeda Laboratory, especially Mari Iwata for technical assistance. We are grateful to Dr. Tsutomu Suzuki and Dr. Minoru Narita at Hoshi University for useful discussion. We thank Dr. Masao Sugamata and Dr. Tomomi Ihara of the Department of Pathology, Institute of Tochigi Clinical Pathology, Inc., Tochigi, for pathological discussion on brain tissue by light and electron microscopy.

This research was supported in part by a Grant-in-Aid for Science Research from Japan Society for the Promotion of Science and a grant from Academic Frontier Project from the Ministry of Education, Culture, Sports, Science and Technology of Japan.

References

[1] M. Block, X. Wu, Z. Pei, G. Li, T. Wang, L. Qin, B. Wilson, J. Yang, J. Hong, B. Veronesi, Nanometer size diesel exhaust particles are selectively toxic to dopaminergic neurons: the role of microglia, phagocytosis, and NADPH oxidase, FASEB J. 18 (2004) 1618–1620.

[2] N. Brose, R. O'Neill, M. Boutelle, S. Anderson, M. Fillenz, Effects of an anxiogenic benzodiazepine receptor ligand on motor activity and dopamine release in nucleus accumbens and striatum in the rat, J. Neurosci. 7 (1987) 2917–2926.

[3] L. Calderón-Garcidueñas, B. Azzarelli, H. Acuna, R. Garcia, T. Gambling, N. Osnaya, S. Monroy, M. DEL Tizapantzi, J. Carson, A. Villarreal-Calderon, B. Rewcastle, Air pollution and brain damage, Toxicol. Pathol. 30 (2002) 373–389.

[4] A. Fujimoto, N. Tsukue, M. Watanabe, I. Sugawara, R. Yanagisawa, H. Takano, S. Yoshida, K. Takeda, Diesel exhaust affects immunological action in the placentas of mice, Environ. Toxicol. 20 (2005) 431–440.

[5] S. Hirano, A. Furuyama, E. Koike, T. Kobayashi, Oxidative-stress potency of organic extracts of diesel exhaust and urban fine particles in rat heart microvessel endothelial cells, Toxicology 187 (2003) 161–170.

[6] T. Ichinose, Y. Yajima, M. Nagashima, S. Takenoshita, Y. Nagamachi, M. Sagai, Lung carcinogenesis and formation of 8-hydroxy-deoxyguanosine in mice by diesel exhaust particles, Carcinogenesis 18 (1997) 185–192.

[7] M. Irifune, T. Sato, T. Nishikawa, T. Masuyama, M. Nomoto, T. Fukuda, M. Kawahara, Hyperlocomotion during recovery from isoflurane anesthesia is associated with increased dopamine turnover in the nucleus accumbens and striatum in mice, Anesthesiology 86 (1997) 464–475.

[8] W. Kim, R. Mohney, B. Wilson, G. Jeohn, B. Liu, J. Hong, Regional difference in susceptibility to lipopolysaccharide-induced neurotoxicity in the rat brain: role of microglia, J. Neurosci. 20 (2000) 6309–6316.

[9] E. Kiyatkin, Functional significance of mesolimbic dopamine, Neurosci. Biobehav. Rev. 19 (1995) 573–598.

[10] M. Konstandi, P. Harkitis, K. Thermos, S. Ogren, E. Johnson, P. Tzimas, M. Marselos, Modification of inherent and drug-induced dopaminergic activity after exposure to benzo(alpha)pyrene, Neurotoxicology 28 (2007) 860–867.

[11] B.W. Laurie RD, Behavioral alterations due to diesel exposure, Environ. Int. 5 (1981) 357–361.

[12] D. Loeffler, A. DeMaggio, P. Juneau, M. Havaich, P. LeWitt, Effects of enhanced striatal dopamine turnover in vivo on glutathione oxidation, Clin. Neuropharmacol. 17 (1994) 370–379.

[13] K. Lundström, J. Tenhunen, C. Tilgmann, T. Karhunen, P. Panula, I. Ulmanen, Cloning, expression and structure of catechol-O-methyltransferase, Biochim. Biophys. Acta 1251 (1995) 1–10.

[14] R. McClellan, Health effects of exposure to diesel exhaust particles, Annu. Rev. Pharmacol. Toxicol. 27 (1987) 279–300.

[15] N. Mills, H. Törnqvist, S. Robinson, M. Gonzalez, K. Darnley, W. MacNee, N. Boon, K. Donaldson, A. Blomberg, T. Sandstrom, D. Newby, Diesel exhaust inhalation causes vascular dysfunction and impaired endogenous fibrinolysis, Circulation 112 (2005) 3930–3936.

[16] P. Männistö, S. Kaakkola, Catechol-O-methyltransferase (COMT): biochemistry, molecular biology, pharmacology, and clinical efficacy of the new selective COMT inhibitors, Pharmacol. Rev. 51 (1999) 593–628.

[17] N. Ono, S. Oshio, Y. Niwata, S. Yoshida, N. Tsukue, I. Sugawara, H. Takano, K. Takeda, Prenatal exposure to diesel exhaust impairs mouse spermatogenesis, Inhal. Toxicol. 19 (2007) 275–281.

[18] M. Sagai, A. Furuyama, T. Ichinose, Biological effects of diesel exhaust particles (DEP). III. Pathogenesis of asthma like symptoms in mice, Free Radic. Biol. Med. 21 (1996) 199–209.

[19] D. Schuetzle, Sampling of vehicle emissions for chemical analysis and biological testing, Environ. Health Perspect. 47 (1983) 65–80.

[20] J.M. Siegel, Brainstem mechanisms generating REM sleep, Princ. Pract. Sleep Med. 3 (2000) 112–133.

[21] M. Strandell, S. Zakrisson, T. Alsberg, R. Westerholm, L. Winquist, U. Rannug, Chemical analysis and biological testing of a polar fraction of ambient air, diesel engine, and gasoline engine particulate extracts, Environ. Health Perspect. 102 (Suppl. 4) (1994) 85–92.

[22] I.T. Sugamat M, H. Takano, S. Oshio, K. Takeda, Maternal diesel exhaust exposure damages newborn murine brains, J. Health Sci. 52 (2006) 82–84.

[23] H. Takano, T. Yoshikawa, T. Ichinose, Y. Miyabara, K. Imaoka, M. Sagai, Diesel exhaust particles enhance antigen-induced airway inflammation and local cytokine expression in mice, Am. J. Respir. Crit. Care Med. 156 (1997) 36–42.

[24] V. Vouk, W. Piver, Metallic elements in fossil fuel combustion products: amounts and form of emissions and evaluation of carcinogenicity and mutagenicity, Environ. Health Perspect. 47 (1983) 201–225.

[25] J. Weimer, J. Benedict, Y. Elshatory, D. Short, D. Ramirez-Montealegre, D. Ryan, N. Alexander, H. Federoff, J. Cooper, D. Pearce, Alterations in striatal dopamine catabolism precede loss of substantia nigra neurons in a mouse model of juvenile neuronal ceroid lipofuscinosis, Brain Res. 1162 (2007) 98–112.

[26] S. Yoshida, M. Sagai, S. Oshio, T. Umeda, T. Ihara, M. Sugamata, I. Sugawara, K. Takeda, Exposure to diesel exhaust affects the male reproductive system of mice, Int. J. Androl. 22 (1999) 307–315.

[27] S. Yoshida, M. Yoshida, I. Sugawara, K. Takeda, Mice strain differences in effects of fetal exposure to diesel exhaust gas on male gonadal differentiation, Environ. Sci. 13 (2006) 117–123.

Toxicology in Vitro 22 (2008) 1825–1831

Contents lists available at ScienceDirect

Toxicology in Vitro

journal homepage: www.elsevier.com/locate/toxinvit

The effects of nanoparticles on mouse testis Leydig cells *in vitro*

Tomoko Komatsu [a], Masako Tabata [a], Miyoko Kubo-Irie [a], Takahisa Shimizu [a], Ken-ichiro Suzuki [b], Yoshimasa Nihei [b], Ken Takeda [a,*]

[a] *Department of Hygiene-Chemistry, Faculty of Pharmaceutical Sciences, Tokyo University of Science, 2641 Yamazaki Noda-shi Chiba, 278-8510, Japan*
[b] *Department of Pure and Applied Chemistry, Faculty of Science and Technology, Tokyo University of Science, 2641 Yamazaki Noda-shi Chiba, 278-8510, Japan*

ARTICLE INFO

Article history:
Received 2 July 2008
Accepted 19 August 2008
Available online 5 September 2008

Keywords:
Leydig cells
Diesel exhaust particles
Titanium dioxide
Carbon black
Nanoparticles

ABSTRACT

We have indicated the possibility that nanoparticles such as diesel exhaust particles (DEP) and titanium dioxide (TiO_2) may impair the male mouse reproductive system. In this study, to evaluate the direct effect of nanoparticles on testis-constituent cells, we examined the effect of DEP, TiO_2 and carbon black (CB) on mouse Leydig TM3 cells, the testosterone-producing cells of the testis. The uptake of three nanoparticles into Leydig cells was detected using transmission electron microscopy (TEM) or field emission type scanning electron microscopy/energy-dispersive X-ray spectroscopy (FE-SEM/EDS). We examined the cytotoxicity and the effect on gene expression by treatment with nanoparticles. TiO_2 was more cytotoxic to Leydig cells than other nanoparticles. The proliferation of Leydig cells was suppressed transiently by treatment with TiO_2 or DEP. The expression of heme oxygenase-1 (HO-1), a sensitive marker for oxidative stress, was induced remarkably by treatment with DEP. Furthermore, CB and DEP slightly increased the gene expression of the steroidogenic acute regulatory (StAR) protein, the factor that controls mitochondrial cholesterol transfer. In this study, we found that DEPs, TiO_2 and CB nanoparticles were taken up by Leydig cells, and affected the viability, proliferation and gene expression. The patterns were unique for each nanoparticle.

1. Introduction

Nanotechnology is an emerging technology, the development of which is expected to impact the fields of information technology, medical treatment, and environmental preservation. Various nanomaterials such as carbon black (CB), titanium dioxide (TiO_2) and fullerene have been developed as basic materials for nanotechnology and their production is increasing. While many of these industrial nanoparticles have been intentionally produced and used, unintentionally produced nanoparticles, such as diesel exhaust particles (DEP), are also discharged into the atmosphere. As a result, people are at increasing risk of exposure to nanoparticles, which enter body through the skin, lungs or the intestinal tract. From there, they are deposited in several organs and may cause adverse biological reactions by modifying the physiochemical properties of living matter at the nano level (Oberdörster et al., 2005a,b). Air pollutants, including DEP have been identified in a number of epidemiological studies as causing adverse health effects, including respiratory and cardiovascular diseases (Atkinson et al., 2001; Pope et al., 1992). Recently, a number of investigators have found nanoparticles responsible for toxicity in different organs (Shvedova et al., 2003; Lam et al., 2004; Kipen and Las 2005; Radomski et al., 2005; Chen et al., 2006; Donaldson et al., 2006; Hussain et al., 2006). It is therefore important to clarify the effects of various nanoparticles on human health as well as the pathogenic mechanisms and signaling pathways involved.

In a previous study, we reported that diesel exhaust (DE), including DEP, influence reproductive function (Yoshida et al., 1999, 2002; Tsukue et al., 2004; Yoshida et al., 2006; Ono et al., 2007). Exposure to DE has been shown in developing mice to induce Leydig cell degeneration, increase the number of damaged seminiferous tubules, and reduce daily sperm production (DSP) (Yoshida et al., 1999). Furthermore, we detected that the effect of DE exposure on male mouse reproductive function is reduced when a high performance filter removes DEP (unpublished data). Recently, we examined the effect of TiO_2 nanoparticles on the mouse reproductive system, where we observed that the nanoparticles decreased DSP per gram of testis and induced abnormalities in the nuclei of spermatids (unpublished data). The results suggest that these nanoparticles impair mouse spermatogenesis; however, the mechanisms underlying nanoparticle-induced male reproductive dysfunctions remain to be elucidated.

Abbreviations: DEP, diesel exhaust particle; TiO_2, titanium dioxide; CB, carbon black; TEM, transmission electron microscopy; FE-SEM/EDS, field emission type scanning electron microscopy/energy-dispersive X-ray spectroscopy; DE, diesel exhaust; DSP, daily sperm production.

* Corresponding author. Tel.: +81 4 7121 3618; fax: +81 4 7121 3784.
E-mail address: takedak@rs.noda.tus.ac.jp (K. Takeda).

0887-2333/$ - see front matter © 2008 Published by Elsevier Ltd.
doi:10.1016/j.tiv.2008.08.009

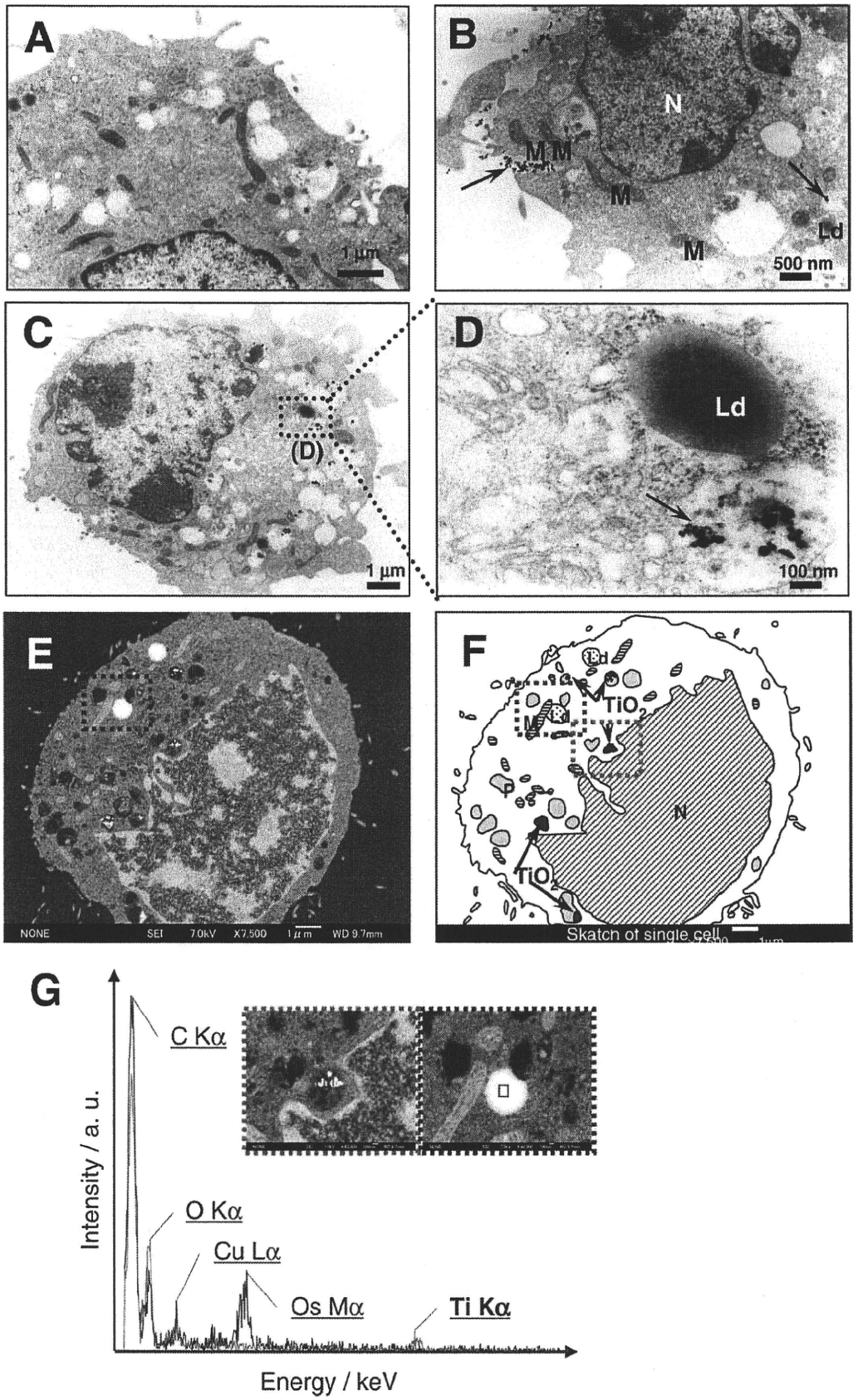

Fig. 1. Thin-section TEM images of TM3 cell incubated with TiO_2. TM3 cells were treated with vehicle only (0.05% Tween 80–0.25% DMSO in PBS) (A) or 30 μg/ml TiO_2 (B, C and D) for 48 h. Identification of TiO_2 nanoparticles in TM3 cells using FE-SEM/EDS (E, F and G). Abbreviations: N, nucleus; M, mitochondria; Ld, lipid droplet; P, phagosome. Arrows denote TiO_2 nanoparticles.

In order to investigate direct reactions of nanoparticles in testis-constituent cells, we examined the effects of nanoparticles on mouse cultured Leydig TM3 cells *in vitro*. The analyzed nanoparticles were DEP, collected from diesel engine; TiO_2, used widely as photocatalytic materials and cosmetics, and CB, produced in the nanotechnology industry. We examined the uptake, intracellular behavior and cytotoxicity of these nanoparticles in the cultured mouse Leydig cells, and compared the differences among the three nanoparticles.

2. Materials and methods

2.1. Cell culture and nanoparticles

The mouse testis Leydig cell line TM3 was purchased from American type Culture collection. The cells were cultured in DMEM F1/2 medium (Life Technologies Inc., Grand Island, NY) supplemented with 2.5% heat-inactivated fetal bovine serum (Filtron Ltd., Victoria, Australia), 5% horse serum (Nacalai Tesque Inc., Kyoto, Japan) and 0.1% gentamicin (Sigma Chemical Co., St. Louis, MO). Incubation was carried out at 37 °C in a humidified 5% CO_2 incubator. The particles used in this study were: (1) TiO_2 (25–70 nm), purchased from Aldrich (St. Louis, MO); (2) CB (14 nm), obtained from Degussa (Essen, Germany) as PrinteX 90; (3) DEP was kindly provided by Dr. Isamu Sugawara (Department of Molecular Pathology, The Research Institute of Tuberculosis). Nanoparticles were suspended in balanced salt solution (0.05% Tween 80–0.25% DMSO in PBS (−)), titrated as stock solutions of 3 mg/ml, and sonicated for 10 min immediately before use in assays.

2.2. Analysis of particle uptake by TEM and FE-SEM/EDS

The cultured cells treated with nanoparticles were fixed with 2.5% glutaraldehyde in 0.2 M sodium cacodylate buffer. After post-fixation in 2% OsO_4 in 0.2 M sodium cacodylate buffer, the samples were dehydrated in ethanol series and embedded in epoxy resin. Morphologic characteristics of the cells and the distribution and agglomeration state of the particles within the cells were investigated using ultra thin sections placed on grids and examined by transmission electron microscopy (TEM). The compositions of nanoparticles in cells were analyzed using field emission type scanning electron microscopy/energy-dispersive X-ray spectroscopy (FE-SEM/EDS).

2.3. Cell viability and proliferation assay

Cells were seeded in 24 well microplates at a density of 1×10^4 cells, incubated for 24 h, and treated with nanoparticles. After incubation for the indicated length of time, the viable cell number was determined by with a hemocytometer using the trypan blue exclusion method.

2.4. Quantitative RT-PCR

Total cellular RNA was isolated using Isogen (Wako, Osaka, Japan). Reverse transcription of total RNA into cDNA was carried out as described elsewhere (Yoshida et al., 2002). Quantitative RT-PCR was performed using a sequence detection system (ABI PRISM 7700; Applied Biosystems, Foster City, CA). Pairs of Primers and TaqMan probes were designed on a computer (Primer Express software; Applied Biosystems) to amplify specific small fragments from HO-1 and StAR. The mouse GAPDH gene was used to provide an internal marker of mRNA integrity. The probe used was a TaqMan MGB probe (Applied Biosystems). PCR amplification was performed in a 96-well optical tray with caps and a 25 μl final reaction mixture consisting of 12.5 μl of TaqMan Universal PCR Mix (Applied Biosystems), 2 μM of TaqMan probe, 3 μM of each primer and cDNA sample. The program conditions were at 95 °C for 10 min, followed by 40 cycles at 94 °C for 15 s and at 60 °C for 1 min.

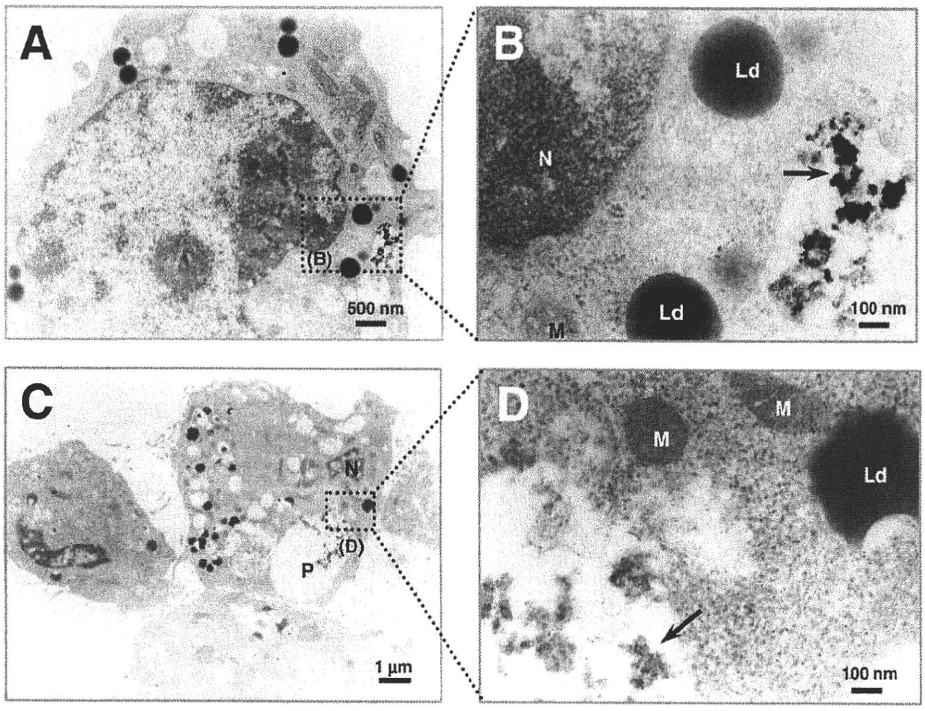

Fig. 2. Thin-section TEM images of TM3 cell incubated with DEP or CB. TM3 cells were treated with 30 μg/ml DEP (A, B) or with 30 μg/ml CB (C, D) for 48 h. Abbreviations: N, nucleus; M, mitochondria; Ld, lipid droplet; P, phagosome. Arrows denote particulate matter.

3. Results

3.1. Cellular uptake of nanoparticles

To investigate whether the different particles were taken up by mouse testis Leydig TM3 cells, we first examined the cells treated with TiO_2 particles for 48 h using TEM. TEM images showed that TiO_2 nanoparticles were taken up by TM3 cells (Fig. 1B–D). TiO_2 nanoparticles were observed in the form of randomly dispersed agglomerates in the cytoplasm. However, the nanoparticles were not closely associated with organelles like the mitochondria. Additionally, the nanoparticles were not observed inside the nucleus. The internalization of TiO_2 nanoparticles into TM3 cells was found after 1–72 h of exposure (data not shown). Additionally, we observed an image that suggested that the internalization occurred through endocytosis (Fig. 1B). To confirm whether or not the nanoparticles observed by TEM contain Ti element, we performed elemental analysis using FE-SEM/EDS (Fig. 1E–G). We compared elemental compositions between the area non-containing the nanoparticles (blue broken rectangle) and the area containing the nanoparticles (magenta broken rectangle) in TiO_2-treated TM3 cells. We detected strong signal of Ti element in the area containing the nanoparticles (magenta line in Fig. 1G). These results indicate that the particles detected in the cells were TiO_2 nanoparticles. Similar results by TEM were obtained for CB nanoparticles and DEP (Fig. 2).

3.2. Effect of nanoparticles on cell viability and proliferation

The effect of DEP, TiO_2 and CB nanoparticles on both cell viability and proliferation was assessed by counting cell numbers with a hemocytometer using the trypan blue exclusion method. To determine whether these particles influence the viability of TM3 cells, the cells were exposed to different concentrations of the three nanoparticles for 48 h. Treatment of TM3 cells with the three nanoparticles resulted in a dose-dependent decrease in the number of viable cells (Fig. 3A). The concentration of 100 μg/ml TiO_2 remarkably inhibited the viability of TM3 cells. In contrast, the same concentrations of DEP and CB (100 μg/ml) did not show a significant effect on the cell viability. This datum shows that TiO_2 nanoparticles are more toxic in TM3 cells than DEP and CB nanoparticles. The effects of the three nanoparticles on cell proliferation of TM3 cells are shown in Fig. 3B. The reductions in cell proliferation were observed for 24 h after treatment at a concentration of 100 μg/ml of TiO_2 or DEP. However, the cell proliferation ability restored after 24 h exposure to TiO_2 or DEP. In contrast, no significant difference existed in the cell proliferation of TM3 cells treated with CB in comparison to non-treated control cells.

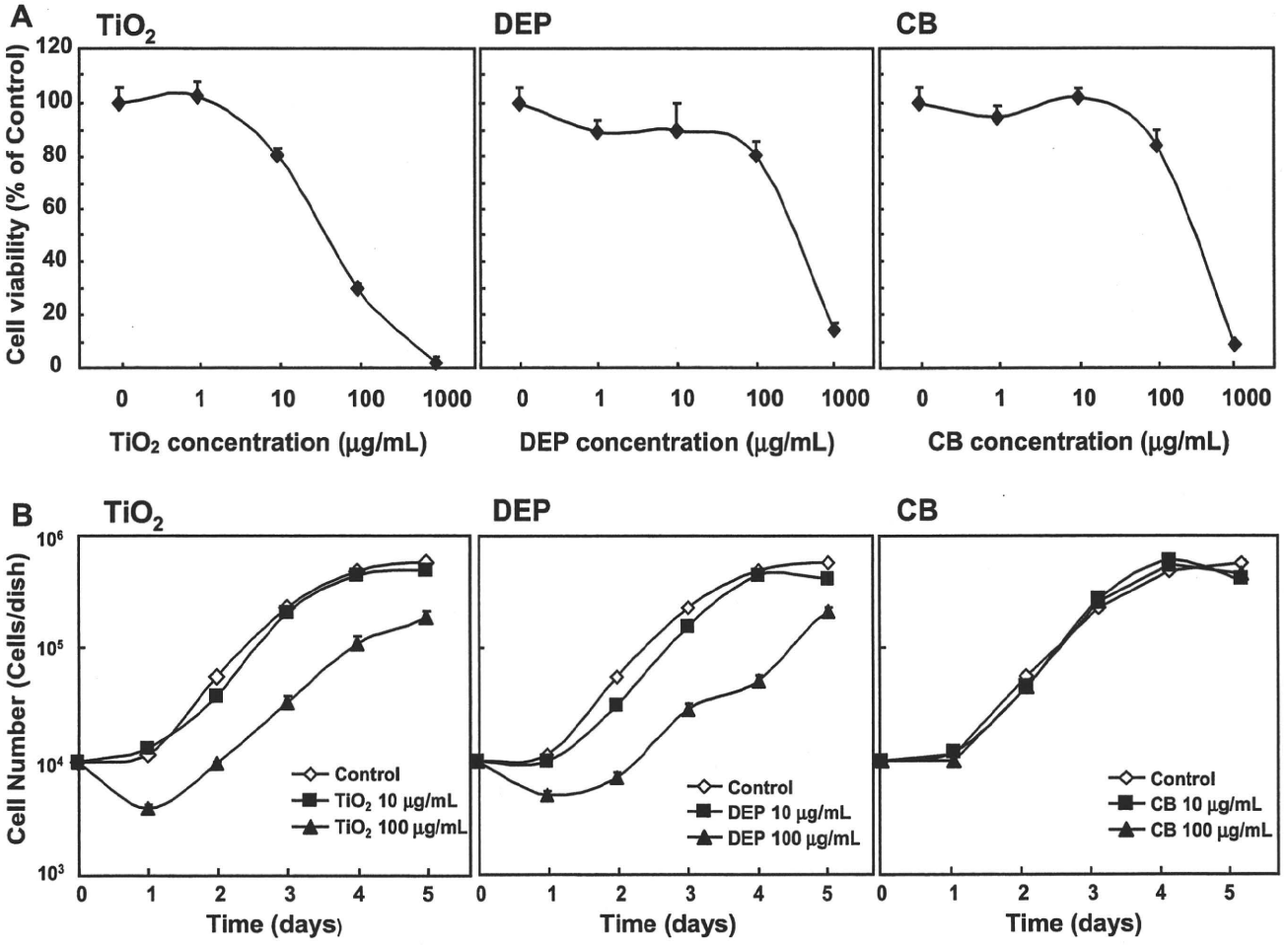

Fig. 3. (A) Dose-dependent effects of DEP, TiO_2 and CB on viability of TM3 cells. Cells were seeded in 24 well microplates (1×10^4 cells/well) for a day, followed by treatment each particles solution (final concentration: 0–1000 μg/ml) for 24 h. Cell viability was determined as described in Section 2. (B) Time-dependent effect of DEP, TiO_2 or CB on proliferation of TM3 cells. Cells were seeded in 24 well microplates (1×10^4 cells/well) for a day, followed by treatment with vehicle only (0.05% Tween 80–0.25% DMSO in PBS) (Control) or each particles (TiO_2, DEP, or CB) for indicated time. The proliferation curve was determined as described in Section 2. Values are means ± S.D. of triplicate determination.

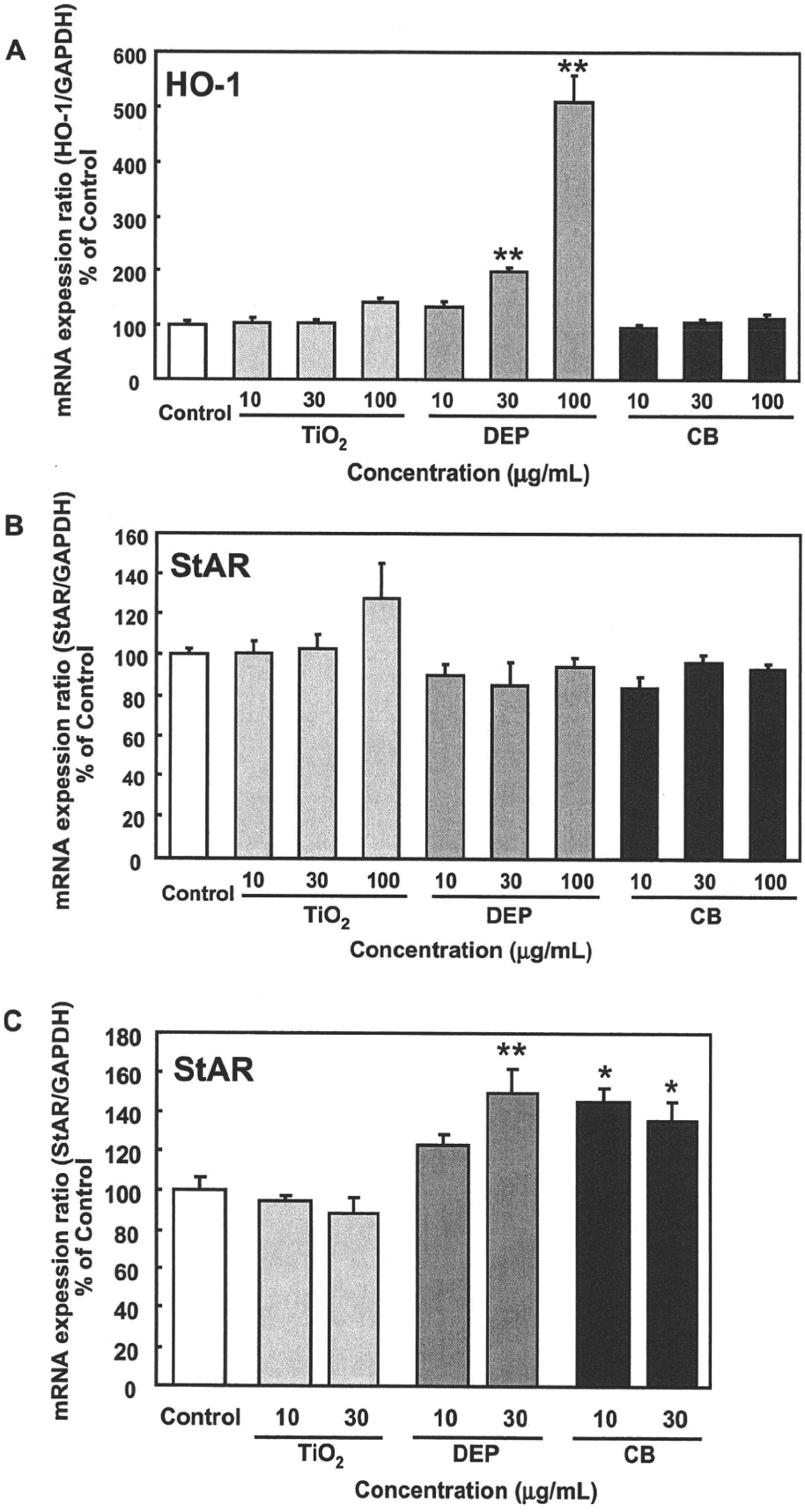

Fig. 4. Expression of HO-1 and StAR mRNAs in TM3 cells treated with DEP, TiO_2 or CB. Total RNA samples were prepared from cells treated with vehicle only (0.05% Tween 80–0.25% DMSO in PBS) (Control) or each particles (TiO_2, DEP, or CB) indicated concentrations for 16 h (A, B) and 48 h (C). Quantitative RT-PCR was performed as described in Section 2. mRNA expression levels are presented as the ratio of HO-1 or StAR mRNA level to GAPDH level in order to correct for variations in the amount of RNA. Ratios were normalized such that the mean ratio of the control was 100%. Values are means ± S.D. of triplicate determination; $^{*}p < 0.05$, $^{**}p < 0.01$.

3.3. Effect of nanoparticles on the expression of HO-1 and StAR mRNA

The expression of the inducible isoform of heme oxygenase-1 (HO-1), which has antioxidant properties, is a very sensitive marker of oxidative stress (due to the fact that its level increases under oxidative stress). To investigate whether nanoparticles induce oxidative stress in Leydig TM3 cells, we examined HO-1 gene expression in TM3 cells treated with TiO_2, DEP and CB using real time RT-PCR (Fig. 4A). HO-1 mRNA expression was increased remarkably in TM3 cells treated with 100 μg/ml DEP for 16 h. In contrast, this effect was not observed in the cells treated with TiO_2 or CB nanoparticles. To examine the effects of nanoparticles on the function of testosterone synthesis in Leydig cells, we analyzed the expression of the steroidogenic acute regulatory (StAR) gene, which is an important molecule in the process of testosterone synthesis. As shown in Fig. 4B, we did not detect a significant effect on StAR expression in TM3 cells treated with TiO_2, DEP or CB for 16 h. Therefore, we examined StAR expression in the cells after 48 h incubation; after which time, enhanced StAR mRNA expression was observed in the cells treated with DEP or CB nanoparticles (Fig. 4C).

4. Discussion

Our study has shown that mouse Leydig cells possess a large capacity for the internalization of DEP, TiO_2 and CB nanoparticles, and that these nanoparticles lead to cytotoxicity and gene expression changes. Additionally, we have shown that there are variations in the effects of these particles. This is the first demonstration of the direct effect of nanoparticles on Leydig cells, the testosterone-producing cells of the testis. We previously indicated the possibility that nanoparticles such as TiO_2 and DEP impair male mouse reproductive system (Yoshida et al., 1999, 2006; Ono et al., 2007). The direct effects of nanoparticles on Leydig cells in this study may represent one mechanism behind the impairment of spermatogenesis in mouse exposed to the nanoparticles.

Uptake of DEP into cells has been reported by several groups. Saxena et al. detected DEP uptake by LA4 lung epithelial cells and MHS alveolar macrophages (Saxena et al., 2008). Two groups indicated that DEP were taken up by human bronchial epithelial cells (Steerenberg et al., 1998; Boland et al., 1999). Furthermore, recent reports have noted the uptake of TiO_2 and CB nanoparticles by several cells including human lung epithelial cells, murine macrophage cells and human vascular endothelial cells (Singh et al., 2007; Xia et al., 2006; Peters et al., 2004; Yamawaki and Iwai, 2006). In addition to these cells, our present results demonstrate for the first time that Leydig cells take up DEP, TiO_2 and CB nanoparticles. We also observed a remarkable reduction of cell viability in TiO_2-treated Leydig cells and transient antiproliferative effects of DEP and TiO_2 in Leydig cells. Many reports reference the effect of DEP, TiO_2 and CB nanoparticles on cytotoxicity in cultured cells *in vitro* (Don Porto Carero et al., 2001; Hussain et al., 2005; Renwick et al., 2001). The effect on cytotoxicity of cells varies among different nanoparticles and among different cells, presumably because of the differing sensibility of cells and the varying sizes and components of particles.

Our results demonstrated that direct exposure of Leydig cells to DEP significantly up-regulates mRNA levels of the oxidative stress marker HO-1; though, TiO_2 and CB nanoparticles have no effect. DEP consist of carbon cores that adsorb many organic compounds including polycyclic aromatic hydrocarbons, heterocyclic organic compounds, quinines, aldehydes, and aliphatic hydrocarbons (Li et al., 2000; Schuetzle et al., 1981; Schuetzle, 1983). DEP and the organic compounds within were shown to induce oxidative and inflammatory effects in lungs, alveolar macrophages, and endothelial cells (Ma and Ma, 2002; Xiao et al., 2003; Hirano et al., 2003). Many groups have reported induction of HO-1 gene expression by the organic extract of DEP in these cells (Li et al.,2000, 2002; Hirano et al., 2003). We indicated that DEP elicit the same action in mouse Leydig cells. It is likely that the induction of the HO-1 gene by DEP in Leydig cells was caused by DEP-adsorbed chemicals rather than particle itself, because CB nanoparticles did not induce HO-1 gene expression in Leydig cells and TiO_2 has no induction effect. This leads us to speculate that oxidative stress is not associated with the cytotoxicity of Leydig cells through TiO_2. In contrast, the expression of StAR gene was induced by DEP and CB nanoparticles in Leydig cells. This result indicates the possibility that these nanoparticles affect the production of steroid hormone in Leydig cells. There are some reports that showed the repression of StAR expression by oxidative stress (Murugesan et al., 2007; Diemer et al., 2003). It has further been reported that the expression of StAR gene was regulated by various transcription factors such as DAX-1, GATA4, C/EBPβ, and AP-1 (Jana et al., 2008; Silverman et al., 2006; Manna et al., 2004). The induction of StAR in Leydig cells by nanoparticles may be associated with these factors.

In summary, the present study examined the direct effects of nanoparticles on mouse Leydig cells in order to investigate the mechanism underlying nanoparticle-induced impairment of spermatogenesis. We observed direct effects of nanoparticles on Leydig cells similar to those seen previously in epitherial cells, macrophages and endotherial cells. Further analysis of the effect leads to the elucidation of mechanism underlying nanoparticle-induced male reproductive dysfunction. Moreover, *in vitro* cultured systems using mouse Leydig TM3 cells may be useful for assessing the effects of injurious matter on spermatogenesis.

Conflict of interest statement

None.

Acknowledgement

This work was supported in part by a Grant-in Aid for Scientific Research from the Ministry of Education, Culture, Sports, Science, and Technology of Japan.

References

Atkinson, R.W., Anderson, H.R., Sunyer, J., Ayres, J., Baccini, M., Vonk, J.M., Boumghar, A., Forastiere, F., Forsberg, B., Touloumi, G., Schwartz, J., Katsouyanni, K., 2001. Acute effects of particulate air pollution on respiratory admissions: results from APHEA 2 project. Air pollution and health: a European approach. American Journal Respiratory and Critical Care Medicine 164, 1860–1866.

Boland, S., Baeza-Squiban, A., Fournier, T., Houcine, O., Gendron, M.C., Chévrier, M., Jouvenot, G., Coste, A., Aubier, M., Marano, F., 1999. Diesel exhaust particles are taken up by human airway epithelial cells in vitro and alter cytokine production. American Journal of Physiology 276, L604–L613.

Chen, Z., Meng, H., Xing, G., Chen, C., Zhao, Y., Jia, G., Wang, T., Yuan, H., Ye, C., Zhao, F., Chai, Z., Zhu, C., Fang, X., Ma, B., Wan, L., 2006. Acute toxicological effects of copper nanoparticles in vivo. Toxicology Letters 163, 109–120.

Diemer, T., Allen, J.A., Hales, K.H., Hales, D.B., 2003. Reactive oxygen disrupts mitochondria in MA-10 tumor Leydig cells and inhibits steroidogenic acute regulatory (StAR) protein and steroidogenesis. Endocrinology 144, 2882–2891.

Don Porto Carero, A., Hoet, P.H., Verschaeve, L., Schoeters, G., Nemery, B., 2001. Genotoxic effects of carbon black particles, diesel exhaust particles, and urban air particulates and their extracts on a human alveolar epithelial cell line (A549) and a human monocytic cell line (THP-1). Environmental and Molecular Mutagenesis 37, 155–163.

Donaldson, K., Aitken, R., Tran, L., Stone, V., Duffin, R., Forrest, G., Alexander, A., 2006. Carbon nanotubes: a review of their properties in relation to pulmonary toxicology and workplace safety. Toxicological Sciences 92, 5–22.

Hirano, S., Furuyama, A., Koike, E., Kobayashi, T., 2003. Oxidative-stress potency of organic extracts of diesel exhaust and urban fine particles in rat heart microvessel endothelial cells. Toxicology 187, 161–170.

Hussain, S.M., Hess, K.L., Gearhart, J.M., Geiss, K.T., Schlager, J.J., 2005. In vitro toxicity of nanoparticles in BRL 3A rat liver cells. Toxicology in Vitro 19, 975–983.

Hussain, S.M., Javorina, A.K., Schrand, A.M., Duhart, H.M., Ali, S.F., Schlager, J.J., 2006. The interaction of manganese nanoparticles with PC-12 cells induces dopamine depletion. Toxicological Sciences 92, 456–463.

Jana, K., Yin, X., Schiffer, R.B., Chen, J.J., Pandey, A.K., Stocco, D.M., Grammas, P., Wang, X., 2008. Chrysin, a natural flavonoid enhances steroidogenesis and steroidogenic acute regulatory protein gene expression in mouse Leydig cells. Journal of Endocrinology 197, 315–323.

Kipen, H.M., Laskin, D.L., 2005. Smaller is not always better: nanotechnology yields nanotoxicology. American Journal of Physiology – Lung Cellular and Molecular Physiology 289, L696–L697.

Lam, C.-W., James, J.T., McCluskey, R., Hunter, R.L., 2004. Pulmonary toxicity of single-wall carbon nanotubes in mice 7 and 90 days after intratracheal instillation. Toxicological Sciences 77, 126–134.

Li, N., Venkatesan, M.I., Miguel, A., Kaplan, R., Gujuluva, C., Alam, J., Nel, A., 2000. Induction of heme oxygenase-1 expression in macrophages by diesel exhaust particle chemicals and quinones via the antioxidant-responsive element. Journal of Immunology 165, 3393–3401.

Li, N., Wang, M., Oberley, T.D., Sempf, J.M., Nel, A.E., 2002. Comparison of the pro-oxidative and proinflammatory effects of organic diesel exhaust particle chemicals in bronchial epithelial cells and macrophages. Journal of Immunology 169, 4531–4541.

Ma, J.Y., Ma, J.K., 2002. The dual effect of the particulate and organic components of diesel exhaust particles on the alteration of pulmonary immune/inflammatory responses and metabolic enzymes. Journal of Environmental Science and Health – Part C: Environmental Carcinogenesis and Ecotoxicology Reviews 20, 117–147.

Manna, P.R., Eubank, D.W., Stocco, D.M., 2004. Assessment of the role of activator protein-1 on transcription of the mouse steroidogenic acute regulatory protein gene. Molecular Endocrinology 18, 558–573.

Murugesan, P., Balaganesh, M., Balasubramanian, K., Arunakaran, J., 2007. Effects of polychlorinated biphenyl (Aroclor 1254) on steroidogenesis and antioxidant system in cultured adult rat Leydig cells. Journal of Endocrinology 192, 325–338.

Oberdörster, G., Maynard, A., Donaldson, K., Castranova, V., Fitzpatrick, J., Ausman, K., Carter, J., Karn, B., Kreyling, W., Lai, D., Olin, S., Monteiro-Riviere, N., Warheit, D., Yang, H., 2005a. Principles for characterizing the potential human health effects from exposure to nanomaterials: elements of a screening strategy. Particle and Fibre Toxicology 2, 8.

Oberdörster, G., Oberdörster, E., Oberdörster, J., 2005b. Nanotoxicology: an emerging discipline evolving from studies of ultrafine particles. Environmental Health Perspectives 113, 823–839.

Ono, N., Oshio, S., Niwata, Y., Yoshida, S., Tsukue, N., Sugawara, I., Takano, H., Takeda, K., 2007. Prenatal exposure to diesel exhaust impairs mouse spermatogenesis. Inhalation Toxicology 19, 275–281.

Peters, K., Unger, R.E., Kirkpatrick, C.J., Gatti, A.M., Monari, E., 2004. Effects of nano-scaled particles on endothelial cell function in vitro: studies on viability, proliferation and inflammation. Journal of Materials Science: Materials in Medicine 15, 321–325.

Pope III, C.A., Schwartz, J., Ransom, M.R., 1992. Daily mortality and PM10 pollution in Utah Valley. Archives of Environmental Health 47, 211–217.

Radomski, A., Jurasz, P., Alonso-Escolano, D., Drews, M., Morandi, M., Malinski, T., Radomski, M.W., 2005. Nanoparticle-induced platelet aggregation and vascular thrombosis. British Journal of Pharmacology 146, 882–893.

Renwick, L.C., Donaldson, K., Clouter, A., 2001. Impairment of alveolar macrophage phagocytosis by ultrafine particles. Toxicology and Applied Pharmacology 172, 119–127.

Saxena, R.K., Gilmour, M.I., Hays, M.D., 2008. Isolation and quantitative estimation of diesel exhaust and carbon black particles ingested by lung epithelial cells and alveolar macrophages in vitro. Biotechniques 44, 799–805.

Schuetzle, D., 1983. Sampling of vehicle emissions for chemical analysis and biological testing. Environmental Health Perspectives 47, 65–80.

Schuetzle, D., Lee, F.S., Prater, T.J., 1981. The identification of polynuclear aromatic hydrocarbon (PAH) derivatives in mutagenic fractions of diesel particulate extracts. International Journal of Environmental Analytical Chemistry 9, 93–144.

Shvedova, A.A., Castranova, V., Kisin, E.R., Schwegler-Berry, D., Murray, A.R., Gandelsman, V.Z., Maynard, A., Baron, P., 2003. Exposure to carbon nanotube material: assessment of nanotube cytotoxicity using human keratinocyte cells. Journal of Toxicology and Environmental Health, Part A 66, 1909–1926.

Silverman, E., Yivgi-Ohana, N., Sher, N., Bell, M., Eimerl, S., Orly, J., 2006. Transcriptional activation of the steroidogenic acute regulatory protein (StAR) gene: GATA-4 and CCAAT/enhancer-binding protein beta confer synergistic responsiveness in hormone-treated rat granulosa and HEK293 cell models. Molecular and Cellular Endocrinology 252, 92–101.

Singh, S., Shi, T., Duffin, R., Albrecht, C., van Berlo, D., Höhr, D., Fubini, B., Martra, G., Fenoglio, I., Borm, P.J., Schins, R.P., 2007. Endocytosis, oxidative stress and IL-8 expression in human lung epithelial cells upon treatment with fine and ultrafine TiO2: role of the specific surface area and of surface methylation of the particles. Toxicology and Applied Pharmacology 222, 141–151.

Steerenberg, P.A., Zonnenberg, J.A., Dormans, J.A., Joon, P.N., Wouters, IM., van Bree, L., Scheepers, P.T., Van Loveren, H., 1998. Diesel exhaust particles induced release of interleukin 6 and 8 by (primed) human bronchial epithelial cells (BEAS 2B) in vitro. Experimental Lung Research 24, 85–100.

Tsukue, N., Yoshida, S., Sugawara, I., Takeda, K., 2004. Effect of diesel exhaust on development of fetal reproductive function in ICR female mice. Journal of Health Science 50, 174–180.

Xia, T., Kovochich, M., Brant, J., Hotze, M., Sempf, J., Oberley, T., Sioutas, C., Yeh, J.I., Wiesner, M.R., Nel, A.E., 2006. Comparison of the abilities of ambient and manufactured nanoparticles to induce cellular toxicity according to an oxidative stress paradigm. Nano Letters 6, 1794–1807.

Xiao, G.G., Wang, M., Li, N., Loo, J.A., Nel, A.E., 2003. Use of proteomics to demonstrate a hierarchical oxidative stress response to diesel exhaust particle chemicals in a macrophage cell line. Journal of Biological Chemistry 278, 50781–50790.

Yamawaki, H., Iwai, N., 2006. Mechanisms underlying nano-sized air-pollution-mediated progression of atherosclerosis: carbon black causes cytotoxic injury/inflammation and inhibits cell growth in vascular endothelial cells. Circulation Journal 70, 129–140.

Yoshida, S., Sagai, M., Oshio, S., Umeda, T., Ihara, T., Sugamata, M., Sugawara, I., Takeda, K., 1999. Exposure to diesel exhaust affects the male reproductive system of mice. International Journal of Andrology 22, 307–315.

Yoshida, M., Yoshida, S., Sugawara, I., Takeda, K., 2002. Maternal exposure to diesel exhaust decreases expression of Steroidogenic Factor-1 and mullerian inhibiting substance in the murine fetus. Journal of Health Science 48, 317–324.

Yoshida, S., Ono, N., Tsukue, N., Oshio, S., Umeda, T., Takano, H., Takeda, K., 2006. In utero exposure to diesel exhaust increased accessory reproductive gland weight and serum testosterone concentration in male mice. Environmental Sciences 13, 139–147.

THE JOURNAL OF BIOLOGICAL CHEMISTRY VOL. 283, NO. 27, pp. 19039–19048, July 4, 2008

Meichroacidin Containing the Membrane Occupation and Recognition Nexus Motif Is Essential for Spermatozoa Morphogenesis*[S]

Received for publication, October 16, 2007, and in revised form, April 29, 2008 Published, JBC Papers in Press, May 3, 2008, DOI 10.1074/jbc.M708590200

Keizo Tokuhiro[‡§], Mika Hirose[‡§], Yasushi Miyagawa[¶], Akira Tsujimura[¶], Shinji Irie[‖], Ayako Isotani[§], Masaru Okabe[§], Yoshiro Toyama[**], Chizuru Ito[**], Kiyotaka Toshimori[**], Ken Takeda[‡‡], Shigeru Oshio[‡‡], Hitoshi Tainaka[‡], Junji Tsuchida[§1], Akihiko Okuyama[¶], Yoshitake Nishimune[§§], and Hiromitsu Tanaka[‡§2]

From the [‡]TANAKA Project, Center for Advanced Science and Innovation, Osaka University, 3-1 Yamadaoka, Suita, Osaka 565-0871, [§]Animal Resource Center for Infectious Diseases, Research Institute for Microbial Diseases, Osaka University, 3-1 Yamadaoka, Suita, Osaka 565-0871, the [¶]Department of Urology, Osaka University Graduate School of Medicine, 3-1 Yamadaoka, Suita, Osaka 565-0871, [‖]Life Science Department, Business Incubation Center, Corporate Manufacturing, Technology, and Research Division, Toppan Printing Company, Ltd., 1-3-3 Suido, Bunkyo-ku, Tokyo 112-8531, the [**]Department of Anatomy and Developmental Biology, Graduate School of Medicine, Chiba University, Chiba 260-8670, the [‡‡]Department of Hygiene Chemistry, Faculty of Pharmaceutical Sciences, Tokyo University of Science, Chiba 278-8510, and [§§]Research Collaboration Center on Emerging and Re-emerging Infections, Research Institute for Microbial Diseases, Osaka University, 3-1 Yamadaoka, Suita, Osaka 565-0871, Japan

Meichroacidin (MCA) is a highly hydrophilic protein that contains the membrane occupation and recognition nexus motif. MCA is expressed during the stages of spermatogenesis from pachytene spermatocytes to mature sperm development and is localized in the male meiotic metaphase chromosome and sperm flagellum. *MCA* sequences are highly conserved in *Ciona intestinalis*, *Cyprinus carpio*, and mammals. To investigate the physiological role of MCA, we generated *MCA*-disrupted mutant mice; homozygous *MCA* mutant males were infertile, but females were not. Sperm was rarely observed in the caput epididymidis of *MCA* mutant males. However, little to no difference was seen in testis mass between wild-type and mutant mice. During sperm morphogenesis, elongated spermatids had retarded flagellum formation and might increase phagocytosis by Sertoli cells. Immunohistochemical analysis revealed that MCA interacts with proteins located on the outer dense fibers of the flagellum. The testicular sperm of *MCA* mutant mice was capable of fertilizing eggs successfully via intracytoplasmic sperm injection and generated healthy progeny. Our results suggest that MCA is essential for sperm flagellum formation and the production of functional sperm.

Haploid cells differentiate only during spermiogenesis following meiosis. The specific features of spermiogenesis include the formation of the tail, mitochondria, and acrosome, nuclear condensation, and the elimination of spermatid cytoplasm. To understand haploid germ cell differentiation fully, *i.e.* spermiogenesis, it is important to identify and characterize specific genes expressed during these developmental processes (1). Meichroacidin (MCA,[3] male meiotic metaphase chromosome-associated acidic protein) was originally isolated using polyclonal antibodies against testicular antigens (2) and is expressed in male germ cells and expressed weakly in the mouse ovary. Specifically, MCA protein is localized predominantly in the cytoplasm of cells throughout the stages of sperm development, *i.e.* from pachytene spermatocytes to round spermatids, as well as in the regions of metaphase chromosomes and spindles during both the first and second meiotic divisions (2). The amino acid sequence of MCA contains a set of seven nominal repeat sequences consisting of the repeat sequence *YXGXX(X)XXXX*-HGQG (2). Recently, junctophilins (JPs), which are a novel conserved family of proteins that are components of the junctional complexes, were reported to contain a repeat amino acid sequence similar to that of MCA (3). However, MCA consists of a hydrophilic amino acid region, whereas JPs have a C-terminal hydrophobic segment spanning the endoplasmic/sarcoplasmic reticulum and are expressed abundantly in a variety of tissues (3, 4). The repeat amino acid sequence, referred to as the membrane occupation and recognition nexus (MORN) motif, is a novel protein-folding module that is shared by functionally different proteins and may have specific physiological roles (3). Southern blots revealed positive bands hybridizing to mouse

* This work was supported in part by grants received from Research and Development to Promote the Creation and Utilization of an Intellectual Infrastructure by the New Energy and Industrial Technology Development Organization of Japan and by the Ministry of Education, Culture, Sports, Science, and Technology of Japan. The costs of publication of this article were defrayed in part by the payment of page charges. This article must therefore be hereby marked "*advertisement*" in accordance with 18 U.S.C. Section 1734 solely to indicate this fact.

[S] The on-line version of this article (available at http://www.jbc.org) contains supplemental Figs. S1–S7 and Tables S1 and S2.

[1] Present address: Dept. of Patho-histocytochemistry, Discovery Research Technologies, Discovery Research Laboratories, Shionogi and Co., Ltd., Sagisu 5-12-4, Fukushima-ku, Osaka 553-0022, Japan.

[2] To whom correspondence should be addressed: Faculty of Pharmaceutical Sciences, Nagasaki International University, Huis Ten Bosch, Sasebo, Nagasaki 859-3298, Japan. Tel./Fax: 81-956-20-5651; E-mail: h-tanaka@niu.ac.jp.

[3] The abbreviations used are: MCA, meichroacidin; MORN, membrane occupation and recognition nexus; JP, junctophilin; SNP, single nucleotide polymorphism; ODF, outer dense fiber; TUNEL, deoxynucleotidyltransferase-mediated dUTP nick end-labeling; PBS, phosphate-buffered saline; FITC, fluorescein isothiocyanate; CTAB, cetyltrimethylammonium bromide; PFA, paraformaldehyde; FS/H, fibrous sheath/head; h, human; Ax, axoneme.

MCA cDNA probes in chromosomal DNA samples from other species, including rats, chickens, *Xenopus*, pufferfish, and humans (2). Recently, the *MCA* homolog of the carp (*Cyprinus carpio*) MORN motif-containing sperm-specific axonemal protein (MSAP) was cloned and characterized (5). *MCA* homologs have been found in organisms ranging from unicellular green algae to mammals through the use of computer-assisted analysis (5). In carp and ascidians (*Ciona intestinalis*), *MSAP* is expressed during late spermatogenesis and accumulates in mature spermatozoa, where it is localized in the basal body and flagellum (5, 6). The isolation and characterization of human *MCA* (*h-MCA*) indicate that h-MCA protein is localized in the sperm flagellum and basal body (7, 8). These results suggest that h-MCA plays an important physiological role in flagellum formation during spermiogenesis.

Here we demonstrated that MCA is expressed in cytoplasm spermatids and is dominantly localized in the outer dense fibers of the flagellum. In addition, mice deficient in MCA exhibit male infertility and azoospermia because of impaired sperm formation. We used single nucleotide polymorphism (SNP) studies to identify two SNPs that induce amino acid substitutions in azoospermic or oligospermic infertile human males. It is possible that SNPs in MCA are related to human infertility.

EXPERIMENTAL PROCEDURES

Animals—All mice were bred and maintained in our laboratory animal facilities and used in accordance with the guidelines for the care and use of laboratory animals set forth by the Japanese Association for Laboratory Animal Science. The mice were kept under controlled temperature and lighting conditions throughout the experiments and were provided with food and water *ad libitum*.

Northern Blots—Total RNA was isolated from various mouse tissues using RNA zolTM B (Invitrogen). Total RNA was extracted according to the manufacturer's instructions and was quantified using optical density measurements. RNA samples containing 2.2 M formaldehyde were electrophoresed in 1.1% agarose gels containing 0.66 M formaldehyde. The RNA was transferred to a nitrocellulose filter in 20× SSC and hybridized with ^{32}P-labeled cDNA prepared using the BcaBest random primer kit (Takara, Shiga, Japan) at 65 °C for 2 h in a PerfectHyb (Toyobo, Osaka, Japan).

Western Blots—Testes freshly removed from mice were homogenized on ice with TBS-T buffer (100 mmol/liter Tris-HCl, pH 7.5, 150 mmol/liter NaCl, 0.2% Tween 20). After centrifugation at 17,800 × *g*, the protein concentration of the supernatant was estimated using a Bradford protein assay (Nacalai, Kyoto, Japan). Following protein quantification, 50 μg of protein from each extract were subjected to SDS-PAGE, followed by electroblotting to a polyvinylidene difluoride membrane (Millipore, Bedford, MA). The membranes were blocked with 5% nonfat dry milk and washed for 15 min with TBS (100 mmol/liter Tris-HCl, pH 7.5, 150 mmol/liter NaCl). They were then incubated with each antibody overnight at 4 °C and washed in TBS once for 3 min and then three times for 5 min each. Finally, the membranes were incubated with peroxidase-conjugated anti-rat or anti-rabbit immunoglobulins (1:500; Amersham Biosciences) for 2 h at 25 °C. After further washing, the reactive bands were visualized on development with the POD staining kit (Wako, Osaka, Japan).

Immunoprecipitation—Testicular fractions were lysed with RIPA (10 mmol/liter Tris-HCl, pH 7.5, 150 mmol/liter NaCl, 0.1% deoxycholic acid, 0.3% SDS, 1% Nonidet P-40, and 0.5 ml/liter protease inhibitor mixture; Nacalai). Each antibody was added to Dynabeads-protein G (Invitrogen), washed once with PBS, and then washed three times with PBS containing 0.01% Tween 20 as per the manufacturer's recommendations. The lysates were then centrifuged at 10,000 rpm for 10 min at 4 °C. Glycerol was added to the supernatants at a concentration of 10%. The Dynabeads-protein G was treated with the lysates at 4 °C overnight and was then washed with PBS containing 10% glycerol and 0.1% Tween 20. SDS sample buffer was added to the Dynabeads-protein G, and each sample was subjected to Western blotting.

Mouse Sperm Protein Fractionation—Sperm was collected from 10 mice using Percoll (9) and was fractionated according to a previously described adapted protocol (10). Briefly, sperm was washed from the epididymis and vas deferens and subjected to three sequential extractions at 4 °C in 500 μl of a solution containing 1% Triton X-100 and 2 mM dithiothreitol in 50 mM sodium borate buffer at pH 9.0 for 40 min each. After each extraction, the samples were centrifuged at 400 × *g* using a Tomy MRX-150 centrifuge (Tomy, Tokyo, Japan), and the supernatants were collected (membrane soluble fractions: M1, M2, and M3). The pellet was washed three times with 50 mM sodium borate buffer and suspended in 500 μl of a solution of 0.6 M potassium thiocyanate (KSCN), 2 mM dithiothreitol, and 50 mM Tris-HCl, pH 8.0, for 2 h at 4 °C. After centrifugation at 800 × *g*, the supernatant was collected (central axoneme (Ax) fraction), and the pellet was extracted overnight at 4 °C in 500 μl of a solution containing 4 M urea, 50 mM Tris-HCl, pH 8.0, and 2 mM dithiothreitol. A final centrifugation at 17,800 × *g* was performed to separate the urea-extracted fraction (urea fraction, ODF). Finally, the resulting nonextracted pellet was washed in borate buffer three times, suspended in sperm extraction buffer (62.5 mM Tris-HCl, pH 6.8, 2% SDS, 10% glycerol, and 5% mercaptoethanol), and sonicated on ice for 10 min (fibrous sheath/head fraction: FS/H). The protein concentration of each fraction (*i.e.* M1, M2, M3, Ax, ODF, and FS/H) was estimated using the Bradford protein assay (Nacalai). Fractions M3, Ax, and ODF were precipitated with 10% trichloroacetic acid. Approximately 20 μg of protein from each fraction was separated by SDS-PAGE in 10% polyacrylamide gels. Western blotting was performed as described above. Control antibodies for the membrane (anti-Izumo1) (11), FS/H (anti-AKAP82) (12), and ODF (anti-Odf1) fractions (13) at a final dilution of 500× were used to verify the extracted proteins.

Immunohistochemistry of Sperm—Mouse sperm from the vas deferens and caudal epididymis suspended in PBS was filtered through a nylon mesh and centrifuged at 400 × *g*. The pellet was then washed in PBS, and a few drops were placed on glass slides and dried at 55 °C for 10 min. The slides were blocked with 10% blocking solution (Nacalai) whole serum in PBS for 30 min at room temperature. The drying and blocking conditions were kept the same for all immunohistochemical procedures. Blocked samples were incubated with anti-MCA antibodies (10

μg/μl IgG) or preimmune serum IgG, both diluted in PBS (1000×), overnight at 4 °C. After one wash, the slides were treated with diluted (1000×) anti-rabbit IgG goat serum conjugated with rhodamine or fluorescein isothiocyanate (FITC) for 1 h at room temperature. The slides were then washed and examined under a fluorescence microscope. Triton X-100- and urea-treated sperm obtained from the fractionation of sperm proteins were also examined immunohistochemically using the same protocol. To visualize individual fibers of the ODF, mature sperm was treated for 1 h at room temperature with a solution containing 10 mM Tris-HCl, 30 mM β-mercaptoethanol, 0.2 mM phenylmethylsulfonyl fluoride, and 0.05% cetyltrimethylammonium bromide (CTAB), which is a cationic detergent that, under reducing conditions, extracts all tail structures except for the Odfs, which are released from the tight native form (14). Co-localization of MCA with Odf2 protein was accomplished by incubating intact and CTAB-treated sperm with anti-MCA antibodies that had been conjugated to rhodamine with an EZ-label rhodamine protein labeling kit (Pierce) for 1 h at room temperature. After a thorough wash in PBS, the samples were incubated with anti-Odf2 rabbit polyclonal antibodies for 2 h at room temperature, washed in PBS, and treated with FITC-conjugated diluted rabbit IgG antibody (2000×) for 1 h at room temperature.

Generation of MCA Targeting Mouse—The *MCA*-targeting construct was created by PCR amplification of a homologous 4-kb 5′ arm and 1-kb 3′ arm using *129Sv* genomic DNA as the template. Targeting at the *MCA* genomic locus resulted in the replacement of exons 1–3 with a neomycin cassette. Two amplified fragments were ligated sequentially into cloning sites on either side of the neomycin resistance gene in the targeting vector backbone. The targeting vector contained the neomycin resistance gene and a thymidine kinase gene, both under the control of the PGK promoter. The vector plasmid was linearized by NotI digestion before electroporation into W9.5 embryonic stem cells. Of 144 G418 gancyclovir-resistant clones that were screened for the targeting event, Southern blotting showed that two had undergone the correct homologous recombination. The two targeted cell lines were injected into C57BL/6J blastocysts, resulting in the birth of male chimeric mice. Highly chimeric males were mated with C57BL/6J wild-type females to generate F_1 offspring, half of which were heterozygous for the targeted allele. The embryonic stem cell lines were injected and produced a high percentage of chimeras that entered the germ line. Heterozygous F_1 males were then crossed with C57BL/6J females to obtain heterozygous F_2 animals. Heterozygous F_2 animals were bred to obtain homozygous mutants or to check the Mendelian inheritance. Eight mice older than 3 months were used to determine the fertility rate. The phenotypic variation was assessed, and biochemical analyses were conducted on samples from at least six individuals.

Southern Blotting and PCR—Genomic DNA was extracted from mouse tails using standard protocols (15). Southern blots were conducted to determine the site of the integration of the gene trap sequence in the *MCA* gene locus and to genotype the mice. A 700-bp probe for genomic Southern blotting was generated by PCR amplification from mouse genomic DNA. Genomic DNA samples (10 μg) were digested with ScaI and electrophoresed in 0.8% agarose gels. Southern hybridizations were carried out using standard protocols (15). The mice were genotyped by PCR using two sets of primers (see supplemental Fig. S1) as follows: one set of primers (5′-GGAGTAGCAAGTGATGTCAGGTCC-3′ and 5′-GAGTAACCTGAGGCTATGGCAGG-3′) to amplify the *Neo* gene and one set of primers (5′-CTATCAAGCAGTTACCAGCCACCC-3′ and 5′-GCAGAGGGAGCGAGGCTCAGCACATGG-3′) for the *MCA* gene.

Morphological and Immunohistochemical Observations—For the histochemical examination, fresh testis samples were embedded in O.T.C. compound embedding medium (Sakura Finetek, Tokyo, Japan) and frozen at −20 °C. Then 8-μm thick sections were prepared using a cryomicrotome (HM 500 OM; Microm, Walldorf, Germany) and fixed with 4% paraformaldehyde (PFA) at 4 °C for 10 min. Alternatively, testis samples were fixed in Bouin's solution for 24 h. After fixation, the samples were embedded in paraffin and sectioned at 8-μm thickness. Deparaffinized sections and frozen sections were incubated with the anti-MCA antibody (10 μg/μl IgG) or preimmune serum IgG, both diluted in PBS (1000×) overnight at 4 °C. After one wash, the slides were treated with diluted (1000×) anti-rabbit IgG goat serum conjugated with horseradish peroxidase for 1 h at room temperature. The slides were then washed and visualized by development with the POD immunostain kit (Wako, Osaka, Japan). Sections were treated with each antibody or stained with hematoxylin and eosin. Morphological identification of spermatogenic cells was based on the criteria of Russell *et al.* (16). The number of seminiferous tubules that sloughed spermatocytes or spermatids into the lumen was counted for 35 tubules of heterozygous or homozygous mutant mice.

For electron microscopy, the testis was perfused with 3% glutaraldehyde in HEPES buffer (10 mM HEPES and 145 mM NaCl). After post-fixation with 1% osmium tetroxide, the testis was embedded in Epon. Selected areas were then sectioned and examined.

Detection of Apoptosis—To identify apoptotic cells, we performed immunostaining with anti-active caspase 3 antibody (Promega, Madison, WI) and terminal deoxynucleotidyltransferase-mediated dUTP nick end-labeling (TUNEL) staining using an *in situ* apoptosis detection kit (Takara) according to the manufacturer's instructions. The number of TUNEL-positive signals was counted for 20 seminiferous tubules of heterozygous or homozygous mutant mice. To identify Sertoli cells, we used anti-GATA 4 antibody (Santa Cruz Biotechnology, Santa Cruz, CA). For immunostaining by anti-active caspase 3 and GATA 4, sections of testis fixed in 4% PFA were treated with an antigen unmasking solution (Vector Laboratories, Burlingame, CA). Immunostaining was performed according to the manufacturer's instructions.

Testicular Sperm Extraction with Intracytoplasmic Sperm Injection (TESE-ICSI)—Testis was placed in cold HEPES-CZB, and the tunica albuginea was removed. The bundles of seminiferous tubules were carefully separated using forceps. The separated tubules were examined under a dissecting microscope. Mature sperm was squeezed out from regions of the tubules that were darkened in the innermost part using forceps (17, 18).

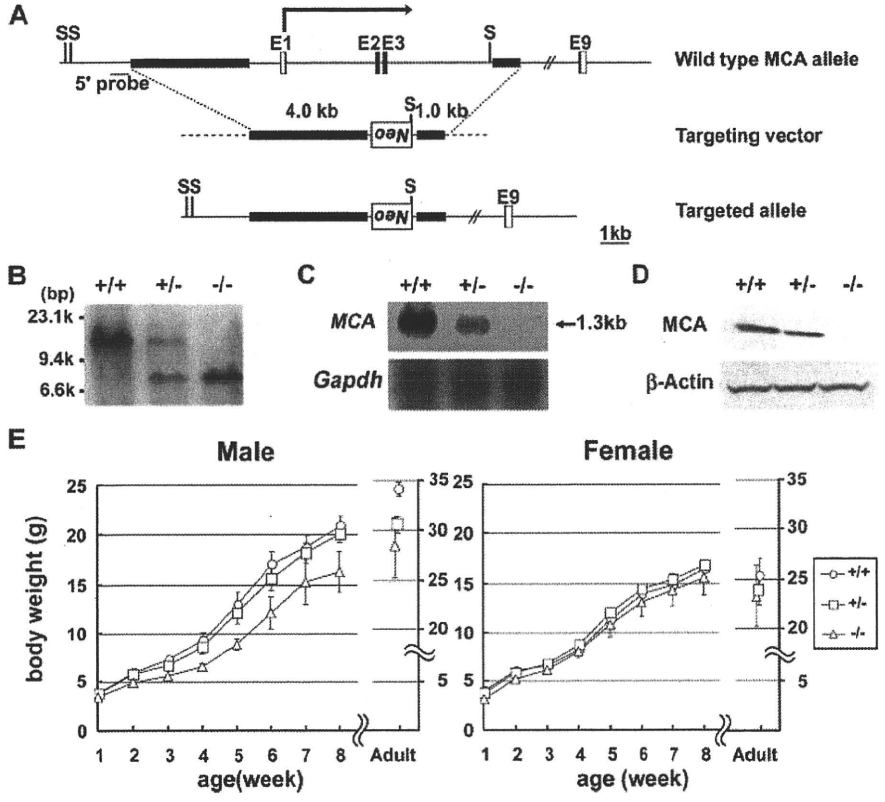

FIGURE 1. **Generation of *MCA* knock-out mice.** *A*, schematic representation of the methods used for gene targeting of the *MCA* genome. The gene targeting construct contains the *Neo* gene (*open box*) between the 4-kb 5′ arm and the 1-kb 3′ arm (*thick lines*). As a result, the regions of exons 1–3 were replaced by the *Neo* gene. Exon 1 includes the first methionine. *Arrows* indicate the transcriptional direction of *MCA*. *S* indicates ScaI restriction sites. *B*, targeted allele was identified by Southern blotting of genomic DNA digested with ScaI using a DNA probe created from the 5′ fragment. *C*, Northern blotting to localize gene expression. *MCA* transcripts are not detectable in the testis of *MCA* homozygous mice. The same membrane was re-hybridized with *Gapdh* cDNA as a control. *D*, Western blotting of testicular lysates of adult mice using an anti-MCA polyclonal antibody. The MCA protein is not detected in the testicular lysate of the homozygous mouse. β-Actin was used as a control. *E*, growth curve of male and female offspring from heterozygous matings (male +/+, $n = 4$; male +/−, $n = 9$; male −/−; $n = 4$; female +/+l $n = 7$; male +/−, $n = 11$; female −/−, $n = 7$).

The sperm was suspended in 12% polyvinyl pyrrolidone in HEPES-CZB and injected into the cytoplasm of unfertilized eggs using a piezo-driven micromanipulator (Prime Tech, Ibaraki, Japan) within 1 h of preparation (19, 20). The injected eggs were cultivated in kSOM (20) overnight and then transferred to the oviducts of pseudopregnant females.

Serum Testosterone—Serum testosterone was measured using an enzyme immunoassay (testosterone enzyme-linked immunosorbent assay kit, catalog number 1880, Alpha Diagnostics, San Antonio, TX).

Identification of SNPs in the Open Reading Frame of MCA—Infertile patients ($n = 245$) were divided into subgroups according to the degree of defective spermatogenesis (21). Of these patients, 153 (68%) had nonobstructive azoospermia and 73 (32%) had severe oligospermia ($<5 \times 10^6$ cells/ml). The control group of fertile males ($n = 172$) included men who had fathered children born at the maternity clinic. DNA samples were extracted from the blood leukocytes of the infertile and proven-fertile males. Genomic DNA was isolated from the blood samples using protease and phenol purification (15). Eight PCR primer sets were designed to amplify the exons of *MCA* genes (see supplemental Tables S1 and S2 and supplemental Fig. S2). PCR was performed using PrimeSTAR or EX Taq hot start (Takara) (see supplemental Table S2). The PCR-amplified fragments were purified using CleanSEQ (Beckman Coulter, Tokyo, Japan), and thermal cycle sequencing (Applied Biosystems, Foster City, CA) was performed. The DNA sequences were determined using the same PCR primers.

Statistical Analysis—Differences between the experimental and control conditions were compared using one-way analysis of variance with Fisher's protected least significant difference tests. Significant differences ($p < 0.05$) are discussed.

RESULTS

MCA Homozygous Mutant Males Are Azoospermic—To investigate the physiological role of MCA, we generated homozygous *MCA* knock-out mice. We constructed the targeting vector (Fig. 1*A*), and homologous recombination was used to generate embryonic stem cell clones that were heterozygous for the *MCA* mutation. To produce chimeric mice, transgenic embryonic stem cells were injected into blastocysts that were subsequently implanted into pseudopregnant mice. We performed Southern blotting to confirm correct recombination (Fig. 1*B*). *MCA* mRNA was not detectable using Northern blots (Fig. 1*C*), and the 40-kDa MCA protein was not detectable using Western blots (Fig. 1*D*) of the testis of homozygous *MCA* mutant mice. Crosses of heterozygous mutant pairs produced the expected ratios of wild-type, heterozygous, and homozygous genotype offspring, according to classical Mendelian inheritance patterns. Homozygous mutant males had slightly smaller body masses than did wild-type males (Fig. 1*E*). Matings between homozygous *MCA* knock-out males and wild-type females did not produce any successful pregnancies during a period of more than 3 months of continuous cohabitation, although vaginal plugs were observed in the paired wild-type females (Table 1). The heterozygous male *MCA* mutant mice and the homozygous females were all fertile (Table 1). Female body mass (Fig. 1*E*), newborn pup growth rates (Fig. 1*E*), and the weights of various organs, including the testes and seminal vesicles of adult *MCA* homozygous mutant mice, did not differ significantly from those of wild-type mice (Table 2). The serum testosterone levels of adult *MCA* homozygous mutant mice were normal compared with those of wild-type mice (Table 2).

MCA Is Essential in Sperm Formation—To confirm the inactivation of *MCA*, an immunohistochemical examination was

TABLE 1
Fertility rates of mutant mice

Genotype	Male fertility (no. of fertile males/no. of vaginal plugs)	Litter size (average no. of newborn pups)[a]	Female fertility (no. of fertile females/no. of vaginal plugs)	Litter size (average no. of newborn pups)[a]
+/−	10/10	8.2 ± 0.3	10/10	7.8 ± 0.3
−/−	0/21	0	8/8	6.0 ± 0.4

[a] Values are means ± S.E.

TABLE 2
Weights of organs, serum testosterone levels, and characteristics of seminiferous tubules in mutant mice
All values are means ± S.E. $n = 6$ mice per genotype.

Parameter	Value for $MCA^{-/-}$ mice	Value for $MCA^{+/-}$ mice	Value for $MCA^{+/+}$ mice
Wet weight of organs/body weight			
Testis	3.3 ± 0.2	3.5 ± 0.2	2.9 ± 0.2
Epididymis	1.5 ± 0.2	1.6 ± 0.1	1.5 ± 0.1
Seminal vesicle	12.7 ± 1.23	12.66 ± 1.45	13.47 ± 1.45
Testosterone level (ng/ml)	1.025 ± 0.730	1.305 ± 1.078	0.917 ± 0.622
Diameter of seminiferous tubules (μm, $n = 8$ tubules per genotype)	165.19 ± 5.82	168.83 ± 4.75	177.14 ± 4.33
No. of cells in seminiferous tubules ($n = 8$ tubules per genotype)	407.8 ± 15.6	421.5 ± 21.6	423.8 ± 15.9

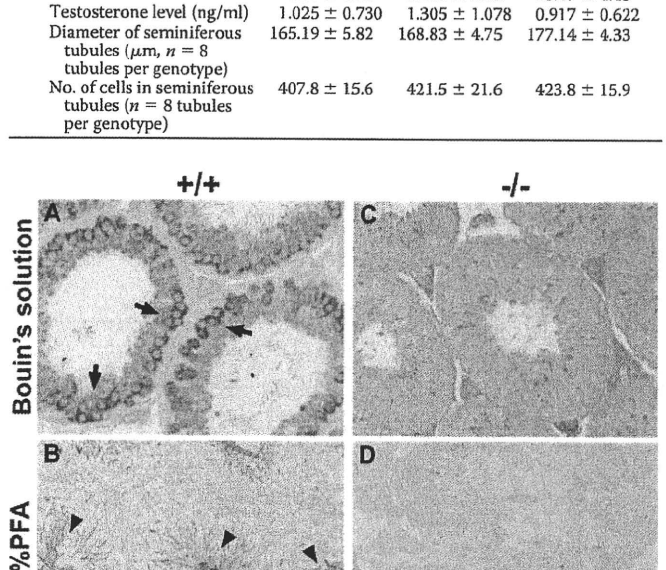

FIGURE 2. **Immunohistochemical staining of the cross-sections of mouse testis with anti-MCA antibody.** The cross-sections fixed in each solution (*left margin*) were incubated with anti-MCA antibody. Cross-sections of wild-type testis (*A* and *B*) or mutant testis (*C* and *D*) are shown. The signals of the cytoplasm of spermatocytes (*arrow*) (*A*) and sperm flagellum (*arrowheads*) (*B*) disappeared in cross-sections of mutant mice (*C* and *D*). *Bar* = 100 μm.

performed. The anti-MCA polyclonal antibody stained some germ cells in testis preserved in Bouin's solution (Fig. 2*A*) (2). The signal was detected in the spermatocytes and elongated spermatids (Fig. 2*A*), and these signals decreased gradually as morphogenesis proceeded, as reported by Tsuchida *et al.* (2). The heat treatment during embedding with paraffin or chemical bonds with the fixative solutions may have altered the exposed sites of the proteins to which the antibodies bound and may have caused the difference in immune staining. To examine the expression of MCA precisely, we performed immunohistochemical analyses using cross-sections preserved in 4% PFA (Fig. 2*B*). The anti-MCA antibody predominantly stained flagella in sperm preserved in 4% PFA (Fig. 2*B*). In *MCA* homozygous mutant males, the signals from testis preserved in either Bouin's solution or 4% PFA disappeared (Fig. 2, *C* and *D*). Rabbit IgG antibody was used as a control (see supplemental Fig. S3). These results indicate that the signals with both types of fixation depend on the *MCA* gene products. In addition, MCA was expressed from the pachytene spermatocyte (stage V) to sperm stages. These observations are in agreement with previous expression profile analyses using Northern and Western blotting (2). MCA might change the conformation in each subcellular localization and play different roles in sperm flagella and the cytoplasm of spermatocytes and spermatids; thus, the difference in conformation might cause different signals for each fixation method.

On microscopic examination, the diameter of the seminiferous tubules and number of cells within the testes of adult wild-type and *MCA* homozygous mutant mice did not differ significantly (Table 2). There were also no significant differences in testis mass between mutant and wild-type mice (Table 2). The spermatogonia, spermatocytes, and spermatids were arranged systematically in the seminiferous tubules in heterozygous mutant testes, just as in wild-type testes; the spermatogonia are located in the tubule walls, and the spermatids are located at the tubule centers, and spermatocytes are located between the two (Fig. 3, *A* and *B*). In mice, the spermatogenic cycle that occurs in each tubule of the seminiferous epithelium is divided into 12 stages (16). In addition, germ cells in the seminiferous tubules are enclosed by Sertoli cells. The spermatocytes or round spermatids had peeled from the Sertoli cells and were found at the tubule centers in ~6% of the seminiferous tubules of mutant testes. Therefore, the arrangement of germ cells in cross-sections was disturbed in *MCA* homozygous mutant testis tubules compared with *MCA* heterozygous mutant testis and wild-type tubules (Fig. 3, *E* and *F*). The epididymides of heterozygous mutant mice were filled with sperm (Fig. 3, *G* and *I*), whereas sperm were sparse or absent in the epididymides of homozygous mutant mice, as observed using light microscopy (Fig. 3, *H* and *J*). *MCA* mutant sperm that was present in the testes had few abnormalities and almost normal head shapes (Fig. 3, *K–P*).

Using electron microscopy, almost all sperm in homozygous *MCA* mutant testes showed abnormalities (Fig. 4 and supplemental Fig. S4), although developed sperm was observed in the seminiferous tubules using light microscopy, and there was no difference in the weights of mutant and wild-type testes (Fig. 3*D* and Table 2). Electron microscopy showed that most spermatids developed normally to step 9 in homozygous mutants (data not shown). However, following nuclear condensation, the rearrangement of mitochondria, and flagellum formation, we observed that the construction of these parts was disturbed, and small vacuoles appeared during spermatid elongation (Fig. 4*A*). Furthermore, the elongated spermatids in homozygous mutant testis were phagocytosed by Sertoli cells (Fig. 4*B* and supple-

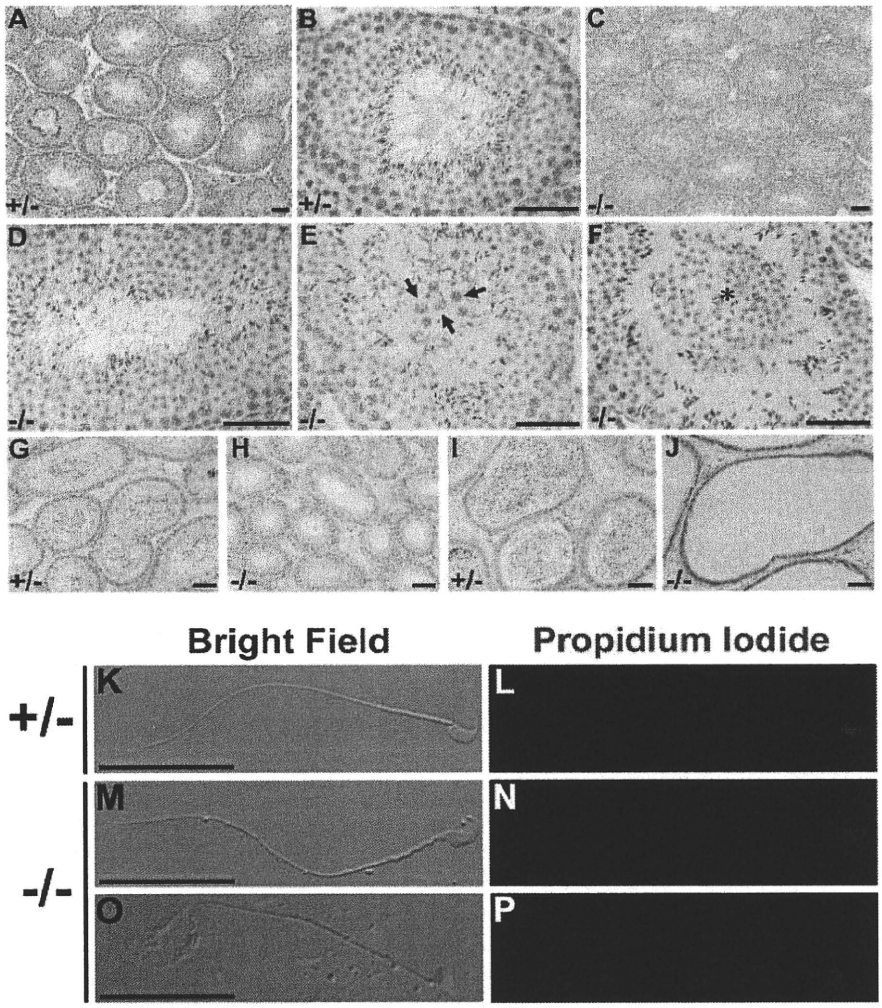

FIGURE 3. **Histological analyses of mutant testis, epididymides, and testicular sperm.** Cross-sections of heterozygous (*A* and *B*) or homozygous mutant (*C–F*) testis are shown. *B* and *D–F* show testicular tubules under high magnification. *Arrows* and an *asterisk* indicate irregularly arranged spermatocytes and round spermatids, respectively. Cross-sections of heterozygous (*G* and *I*) or homozygous mutant (*H* and *J*) epididymides are shown. *G* and *H* show caput epididymides and *I* and *J* show cauda epididymides. Sperm was not found in homozygous mutant epididymides (*H* and *J*). Heterozygous (*K* and *L*) and homozygous mutant (*M–P*) testicular sperm were observed. The heads of the homozygous mutant sperm have some abnormal features (*O* and *P*). *Bar* = 50 μm.

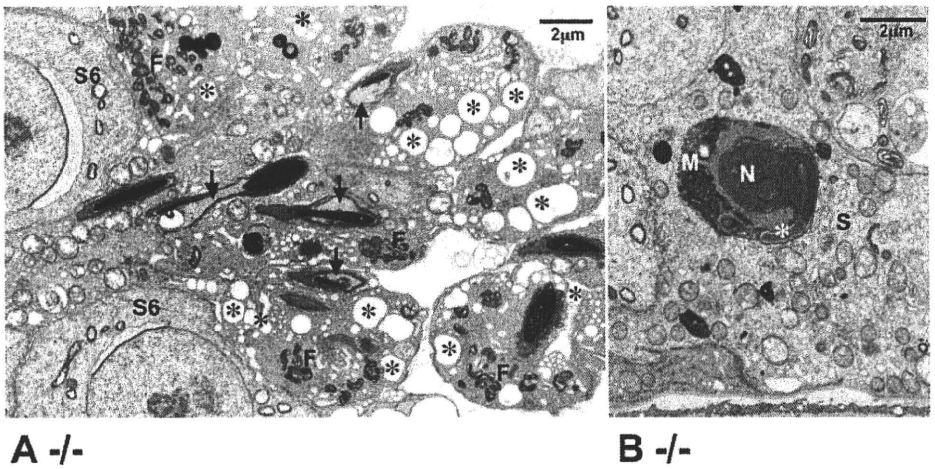

FIGURE 4. **Electron micrographs showing the degeneration of spermatids.** Sections of *MCA* homozygous mutant testis are shown. *A*, spermatids in a stage VI seminiferous tubule. Step 15 spermatids show deformation of the heads (*arrow*) and numerous vacuoles (*) in the cytoplasm. Flagella (*F*) that contain an axoneme, mitochondria, outer dense fibers, and fibrous sheaths are formed; however, these components are disarranged in the cytoplasm. Step 6 spermatids (*S6*) appear to be normal in shape. *B*, spermatid phagocytosed by Sertoli cells (*S*). The highly deformed nucleus/head (*N*), acrosome (*), and mitochondrial sheath (*M*) of the spermatids are shown.

mental Fig. S4). These findings indicate that the absence of *MCA* expression leads to abnormalities in spermatid formation, which in turn results in the abnormal morphogenesis of other components of the sperm. Alternatively, the MCA protein may affect various aspects of sperm morphogenesis directly.

MCA Was Strongly Associated with the ODF—Western blots of the subcellular fractions of sperm proteins indicated that MCA expression was present predominantly in the flagellum and more weakly in the sperm head (Fig. 5*A*). We also performed subcellular fractionation of sperm proteins located in the membrane/cytoplasm, axoneme, ODF, and FS/H. Soluble fraction and the final FS/H-insoluble fractions were separated by SDS-PAGE, transferred to a membrane, and subjected to Western blotting with anti-MCA antibody. MCA was weakly eluted in the membrane fraction that solubilized with a nonionic detergent (Triton X-100) but was mostly solubilized with potassium thiocyanate and urea (Fig. 5*B*). The majority of MCA was indeed recovered in the axoneme and ODF fraction, although a small amount of MCA remained in the nonextracted pellet that contained FS/H fractions (Fig. 5*B*). Izumo sperm-egg fusion 1 (Izumo1) (11) and AKAP82, the major protein of the fibrous sheath of the sperm flagellum (12), were present in the membrane and FS fractions, respectively. Odf1, the major ODF protein (13), was extracted only with urea (Fig. 5*B*). MCA was extracted together with the cytoskeletal elements that make up the axoneme, ODF, and FS.

To examine MCA-protein complexes, immunoprecipitation was performed. In immunoprecipitating complexes of testicular lysate with anti-Odf1, Odf2, and SHIPPO 1/Odf3, MCA co-precipitated with anti-Odf1 and Odf2 (Fig. 5*C*). Furthermore, we examined protein complexes with Septin 4 and Septin 7 (Fig. 5*C*) (22). No signals were detected in protein complexes with these annulus proteins. In addition,

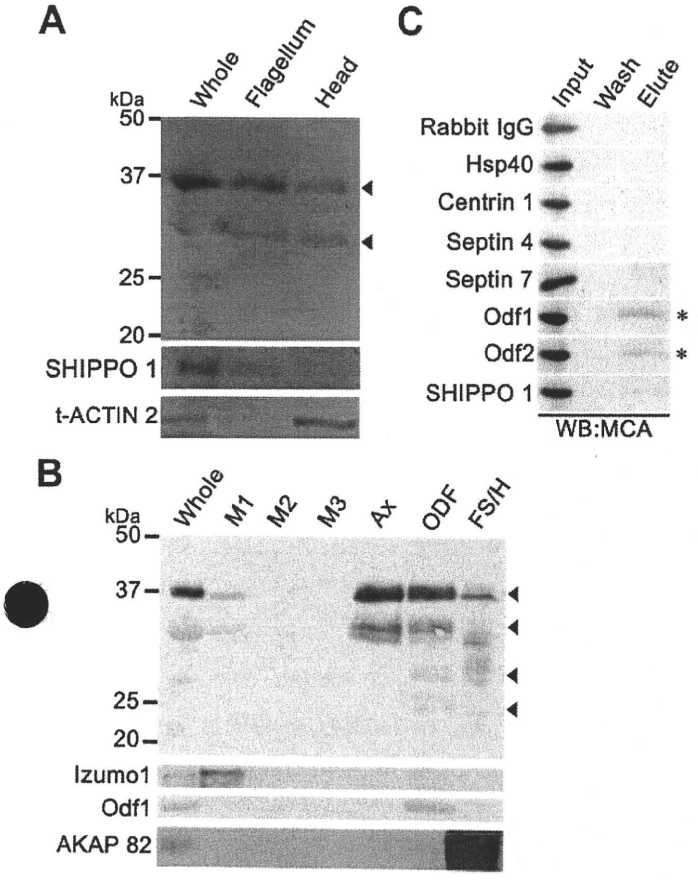

FIGURE 5. **Western blotting of the subcellular fractionation of sperm.** *A*, sperm was sonicated in PBS and fractionated by centrifugation. The *numbers* in the *left margin* indicate the molecular weights of the marker proteins. Anti-SHIPPO 1 or t-ACTIN 2 antibodies were used as controls in the flagellum or sperm head fractions (24, 37). *Arrowheads* indicate the signal of MCA. *B*, whole sperm fractions extracted with SEB. Approximately 20 μg of solubilized protein in each of the fractions obtained by sequential extraction with 1% Triton X-100 (*M1*, *M2*, and *M3*), potassium thiocyanate (*Ax*), and urea (*ODF*), and the remaining pellet (*FS/H*) extracted with SEB were tested for the presence of a sperm membrane protein (*Izumo1*), an FS component (*AKAP 82*), and an ODF protein (*Odf1*). Molecular weight marker bands are shown at the *left*. *Arrowheads* indicate the signal of MCA. *C*, lysate of testicular germ cells was immunoprecipitated with antibodies against flagellar proteins. Each antibody is indicated in the *left margin*. The Dynabeads-protein G treated with each antibody was reacted with the lysate (*Input*). After washing (*Wash*), the protein complexes were eluted from the Dynabeads using elution buffer (*Elute*). Each fraction was subjected to SDS-PAGE and Western blotting (*WB*) with anti-MCA antibodies. The *asterisk* indicates significant signals.

MCA was not detected in immunocomplexes with Hsp40 flagellum protein (6) and testis-specific centriole protein (*Centrin 1*, Fig. 5*C*) (23).

To examine the subcellular localization of MCA in detail, its presence in sperm treated with 0.05% CTAB and in samples from fractionation experiments following 1% Triton X-100 and 4 M urea treatment was determined using immunocytochemistry. Nontreated sperm displayed basic staining patterns for MCA (Fig. 6, *A–C* and see supplemental Fig. S5); the entire length of the sperm flagellum was stained homogeneously, and the sperm heads were stained weakly. In sperm treated with 1% Triton X-100, the membranes, organelles (including the mitochondrial sheath in the midsection), and cytosolic proteins are solubilized (24). These changes cause the sperm heads to bend because of the weakened support of the neck. In addition, the ODFs are sometimes observed to protrude from the weakened annulus region (10). In Triton X-100-treated sperm, the MCA signal was observed in the fibers along the rest of the flagellum and disappeared from the heads (Fig. 6, *D–H*, and see supplemental Fig. S5 in the supplemental materials). Therefore, MCA is associated with the ODF. As determined by fractionated Western blotting, the treatment of sperm with 4 M urea efficiently extracted most of the ODF protein together with MCA from the sperm flagellum. After only 15 min of exposure to urea, the MCA signal became scattered, and the fiber-like view of MCA in liberated ODF was lost (Fig. 6, *I–K*). Following 30 min of CTAB treatment, sperm released individual ODFs that were freed from the central core of the tail and dispersed distally to the connecting piece. Most sperm heads were separated from the tail, and resistant ODFs were frayed completely and joined together only at the connecting piece (14). MCA and Odf2 signals were clearly observed in individual fibers and the connecting piece (Fig. 6, *L–S*). Therefore, MCA is associated with ODFs and the connecting piece in a nonionic detergent-resistant form (Triton X-100). The MCA signal also appeared in the fibrous proteins that constitute the ODF, following exposure to an ionic detergent (CTAB).

Abnormal Sperm Might Be Phagocytosed by Sertoli Cells—The mass of *MCA* homozygous mutant testis was normal compared with that of wild-type mice (Table 2). However, there was no sperm in the epididymis of mutants. We also examined apoptotic cells in the testis. Apoptosis signals did not increase in germ cells, as determined by the detection of caspase-3 antibody (Fig. 7*A*). There were 0.33 ± 0.19 (average ± S.E.) and 0.20 ± 0.11 positive cells/tubule detected in the testes of homozygous and heterozygous mice, respectively. All cells in the centers of seminiferous tubules and Leydig cells were stained uniformly in testis sections of heterozygous and homozygous mutants. Therefore, these signals resulted from nonspecific staining. Using the TUNEL method, in the testes of heterozygous and homozygous mice, 0.15 ± 0.08 and 0.70 ± 0.19 TUNEL-positive cells/tubule, respectively, were detected (Fig. 7*B*). TUNEL-positive cells increased slightly in the germ cells of the homozygous mutant. There were 5.00 ± 0.75 strong signals with the shape of sperm nuclei per seminiferous tubule detected near the tubule walls, but not in the center, in the homozygous mutant mice only (Fig. 7*B*). The signal visualized using the TUNEL method was located near the nuclei of sperm in Sertoli cells (see supplemental Fig. S6). This signal may indicate the degraded products of sperm nuclei that were phagocytosed by Sertoli cells. *MCA* mutant sperm in the testis did not undergo apoptosis, but might be instead phagocytosed by Sertoli cells.

Sperm of MCA Mutant Mice Can Produce Viable Embryos—MCA was expressed from the spermatocyte through to sperm stages and was localized in meiotic metaphase chromosomes during meiosis (2). We examined whether the nuclei of *MCA* mutant sperm maintained the ability to produce viable embryos using testicular sperm extraction and intracytoplasmic sperm injection (TESE-ICSI). Sperm derived from heterozygous and homozygous *MCA* mutant mice was injected into eggs. Two-cell-stage embryos produced from heterozygous (n = 36) or

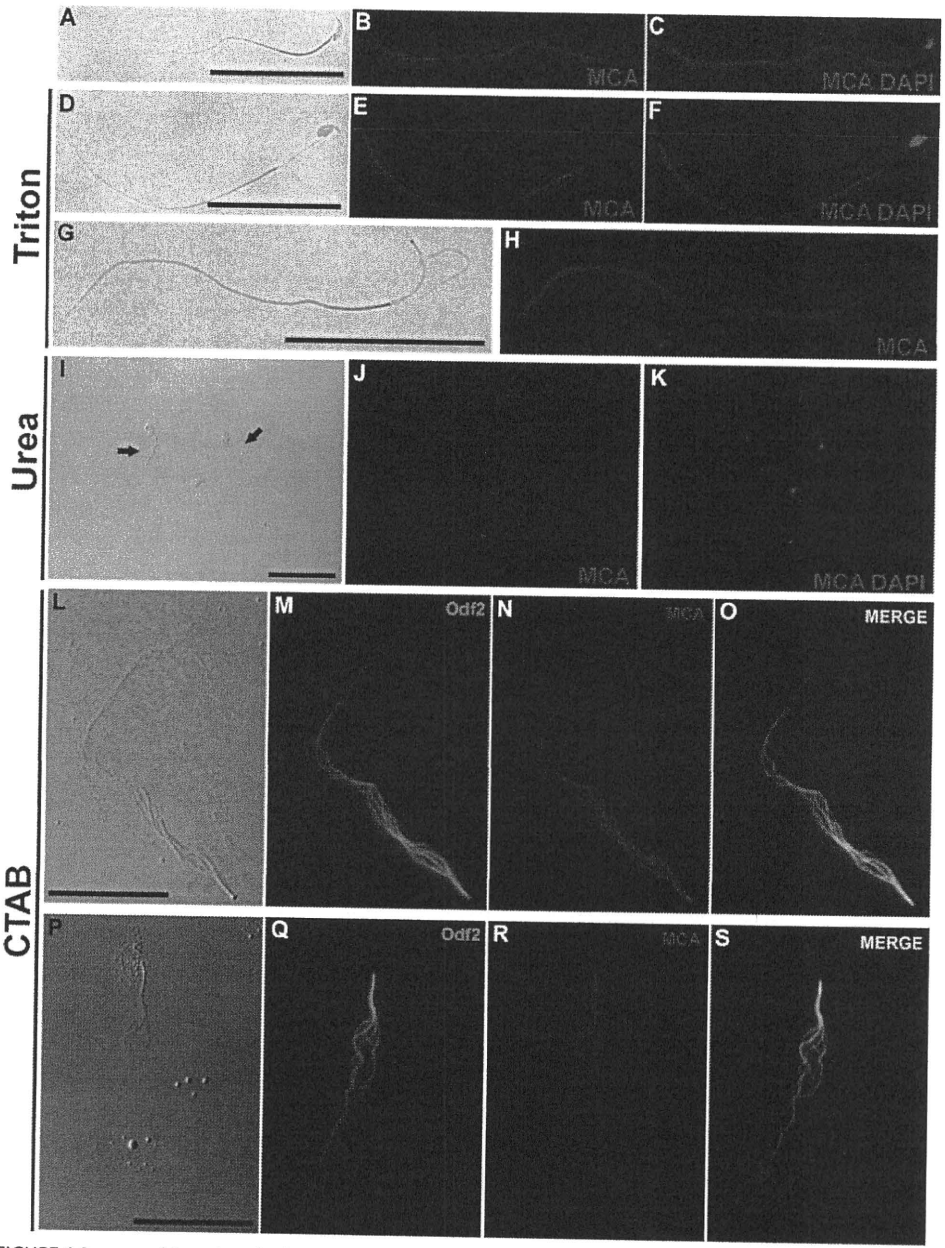

FIGURE 6. **Immunohistochemical examination of MCA in sperm.** Sperm and flagella from the cauda epididymis were stained with anti-MCA antibody (*A–C*). Following treatment with Triton X-100, the MCA signal disappeared from the sperm head but was maintained in the insoluble fractions of the flagellum (*D–H*). The signal disappeared from flagella subjected to urea treatment (*I–K*). Sperm treated with 0.05% CTAB to release the outer dense fibers (*L–S*) were stained with rhodamine-conjugated anti-MCA antibody (*N* and *R*). Samples were also reacted with anti-Odf2 antiserum and stained with FITC-conjugated secondary antibodies (*M* and *Q*). MCA signal was co-localized with Odf2 (*O* and *S*). *Bars* = 50 μm (*A–K*) or 25 μm (*L–S*).

homozygous ($n = 31$) *MCA* mutant sperm were transferred to the oviducts of pseudopregnant females. Nineteen (52%) and 10 (33%) pups were born from heterozygous and homozygous *MCA* mutant sperm, respectively, indicating that the nuclei of *MCA* mutant sperm were as capable of producing viable embryos as those of heterozygous sperm from fertile males.

SNPs in Human MCA—The analysis of human *MCA* sequences in more than 200 infertile male patients and in 172 proven-fertile male volunteers revealed two amino acid substitution-causing SNPs in the open reading frame of *MCA*. These SNPs were found in exon 2 in two of the azoospermia-infertile and in one of the oligospermia-infertile patients (Table 3 and see supplemental Fig. S2). The *a92c* SNP at amino acid 31, located within the first MORN motif in the N-terminal region, was found in three cases of heterozygosity and caused a shift from histidine to proline. The *g121a* SNP at amino acid 41, located between the first and second MORN motifs, was found in one case of heterozygosity and caused a shift from glycine to arginine. The *g393a* SNP in exon 5 at alanine 131 did not induce an amino acid substitution as seen by Rs2839536 in the dbSNP data base of the National Center for Biotechnology Information (NCBI). The prevalence of the *g393a* SNP was similar in proven fertile and infertile patients (Table 3).

DISCUSSION

In this study, we showed that the germ cell-specific *MCA* gene is essential for spermiogenesis and that two different SNPs in the human *MCA* gene (*h-MCA*) are associated with male infertility. A hydropathy plot (25) of the deduced MCA sequence revealed that MCA contains strongly hydrophilic regions throughout its total length (2). MCA is expressed predominantly in the cytoplasm of cells through a variety of stages, ranging from pachytene spermatocytes to sperm. MCA in sperm is localized throughout the cytoplasm and is specifically concentrated in the fibrous sheath (FS) and ODF of the flagellum. Apart from the axoneme and its associated proteins, the sperm flagellum consists of two exclusive cytoskeletal components as follows: the FS in the principal piece and the ODFs in the middle and principal pieces. Nine ODFs are anchored proximally at the connecting piece and run parallel to the tubulin doublets of the axoneme toward the distal end of the flagellum. Longitudinal columns and transversal ribs of the FS surround the ODF in the principal piece (26). The majority of proteins in the ODF and FS are hydrophobic and resist solubilization by ionic detergents (*e.g.* SDS) (10, 27, 28). Many proteins that were localized in this area have been identified previously (29). Of these proteins, glyceraldehyde-3-phosphate dehydrogenase-S was predominantly localized in the FS; however, it may be active only in the hydrophilic state

(30). There is little information available on how the hydrophilic FS and ODF are assembled in developing spermatids and how proteins in the FS and ODF maintain their functions. Even the hydrophilic protein MCA can occur in the FS and ODF, although it may be modified. Interactions between MCA and other proteins may support flagellum function and development.

MCA contains a set of seven MORN motifs. JPs, which are components of the junctional complexes that are expressed abundantly in the heart and brain, contain a conserved MORN motif (3, 4). The MORN motifs of JPs have tandem repeats of eight MORN motifs at the N-terminal region and a hydrophobic domain in the C-terminal region, which may function in anchoring the protein to the cellular membrane (see supplemental Fig. S7) (3). Other proteins containing a few MORN motifs have also been reported (see supplemental Fig. S7). MORN motifs may play an important role in protein complexes; however, the exact function of the MORN motif is not clear. The localization of the MORN motif in MCA was not significantly different from that in JPs. The exact function of the MORN motif may be more noticeable in MCA that consists of the MORN motif only.

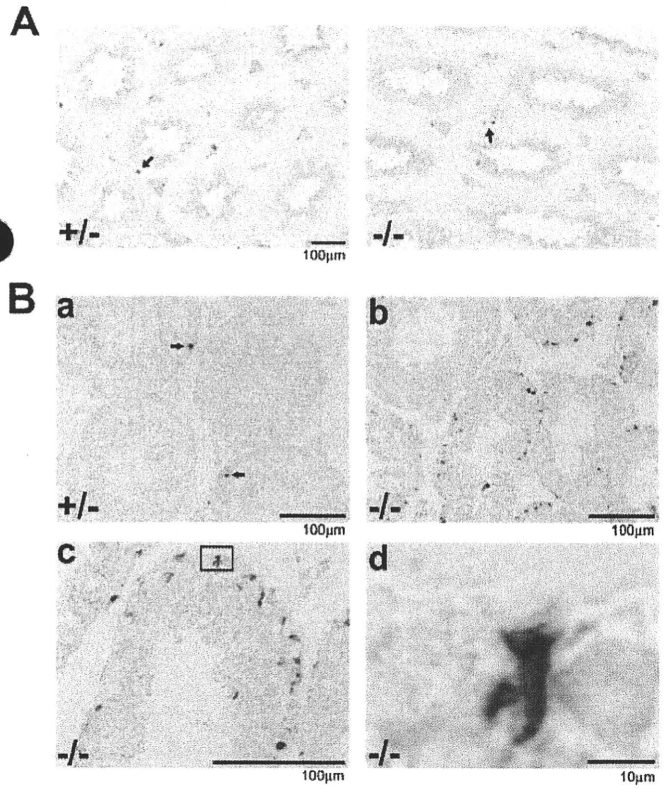

FIGURE 7. **Occurrence of apoptosis in the testis.** *A*, expression of active caspase 3 was observed in heterozygous (+/−) and homozygous (−/−) mutant mouse testis. *Arrows* indicate germ cells expressing active caspase 3. Cells in the centers of the tubules and Leydig cells were stained nonspecifically. *B*, TUNEL staining was performed on sections of testis. Apoptotic signals were observed in heterozygous mutant testis (*arrows*) (*panel a*). Signals indicated that phagocytosed cells were observed in the tubule walls of homozygous mutants (*panels b–d*). *Panels c* and *d*, high magnification of the signals found in mutant testis. *Panel d*, high magnification of the *box* in *panel c*.

Sperm in the testis of mutant mice appeared normal under light microscopy; however, detailed analysis using electron microscopy revealed some abnormalities. In other gene mutational mice that display abnormal sperm formation, sperm is sent to the epididymis even if it is abnormal (31). In addition, the abnormal sperm is observed in the vaginal plugs. However, the *MCA* mutant mice were azoospermic, and most defective sperm might be phagocytosed by the Sertoli cells. The absence of sperm in the epididimydis can be at least partly explained by Sertoli cell phagocytosis of defective sperms.

In the rat, epididymal ligation causes extensive degeneration of the seminiferous epithelium with loss of virtually the entire germ cell population and a significant decline in both testicular and epididymal weight (32), although ligation of the initial segment of the caput epididymis results in temporary testicular changes followed by evidence of recovery in the mouse (33). These testicular alterations differed from that of the *MCA* mutant testes. Furthermore, a few abnormally shaped sperm heads were occasionally observed in the cauda epididymis using light microscopy (data not shown). *MCA* mutant mice were nonobstructive azoospermic, although the relative size of the testis was normal. SNPs in the MORN motif of MCA only occurred in infertile men. These SNPs were heterozygotes of the major and minor SNP. *DMC1* is a *RecA* homolog that is specifically expressed during meiosis and is thought to play an important role. When one allele is not expressed in the DMC1 protein, the dysfunction does not appear (34). However, abnormal meiosis occurs when the mutant DMC protein is expressed from another allele (35). The male infertility-specific SNPs that we found may cause male infertility through their effects on mutant MCA protein expression. The *a92c* SNP may cause male infertility more readily than does the wild-type MCA and

TABLE 3
Prevalence of *MCA* SNPs in infertile and proven-fertile human populations

Exon	Position[a]			Genotype	No. of SNP				Reference (NCBI dbSNP)
	Nucleotide	Amino acid			Infertile		Proven fertile		
						%		%	
Exon 2	92	31	(H)	A/A	242	(99)	172	(100)	
			(H/P)	A/C	3	(1)	0	(0)	
			(P)	C/C	0	(0)	0	(0)	
	121	41	(G)	G/G	244	(99.5)	172	(100)	
			(G/R)	G/A	1	(0.5)	0	(0)	
			(R/R)	A/A	0	(0)	0	(0)	
Exon 5	393	131	(A)	G/G	141	(62)	82	(62)	
			(A)	G/A	79	(35)	41	(31)	Rs2839536
			(A)	A/A	7	(3)	9	(7)	
				ND[b]	20		40		

[a] Translation start site was +1.
[b] G393A haplotype in exon 5 was not decided exactly in 20 and 40 persons of infertile or proven fertile group, respectively.

may be transferred to the next generation via the female, as indicated by the results of the *MCA* mutant mouse study. Approximately 15% of couples that attempt to conceive over a 2-year period are unable to become pregnant (36). Recent technological developments in *in vitro* fertilization have ensured that even when sperm activity is low, pregnancy and birth are possible. The molecular mechanisms behind infertility remain uncertain. It is possible that SNPs in MCA are related to human infertility.

Collectively, our results demonstrate that MCA proteins containing the MORN motif play an important role in the construction of hydrophobic protein complexes in the sperm flagellum. These findings are valuable not only for understanding the molecular mechanisms of spermiogenesis but also for determining the function of proteins encoded by the MORN motif.

Acknowledgments—We thank Mayumi Ikenishi, Lina Fujita, and Mitsuko Yokota for technical assistance.

REFERENCES

1. Nishimune, Y., and Tanaka, H. (2006) *J. Androl.* **27,** 326–334
2. Tsuchida, J., Nishina, Y., Wakabayashi, N., Nozaki, M., Sakai, Y., and Nishimune, Y. (1998) *Dev. Biol.* **197,** 67–76
3. Takeshima, H., Komazaki, S., Nishi, M., Iino, M., and Kangawa, K. (2000) *Mol. Cell* **6,** 11–22
4. Moriguchi, S., Nishi, M., Komazaki, S., Sakagami, H., Miyazaki, T., Masumiya, H., Saito, S. Y., Watanabe, M., Kondo, H., Yawo, H., Fukunaga, K., and Takeshima, H. (2006) *Proc. Natl. Acad. Sci. U. S. A.* **103,** 10811–10816
5. Ju, T. K., and Huang, F. L. (2004) *Biol. Reprod.* **71,** 1419–1429
6. Satouh, Y., Padma, P., Toda, T., Satoh, N., Ide, H., and Inaba, K. (2005) *Mol. Biol. Cell* **16,** 626–636
7. Matsuoka, Y., Nishimura, H., Numazawa, K., Tsuchida, J., Miyagawa, Y., Tsujimura, A., Matsumiya, K., Okuyama, A., Nishimune, Y., and Tanaka, H. (2005) *Rep. Med. Biol.* **4,** 213–219
8. Shetty, J., Klotz, K. L., Wolkowicz, M. J., Flickinger, C. J., and Herr, J. C. (2007) *Gene (Amst.)* **396,** 93–107
9. Bellve, A. R., Zheng, W., and Martinova, Y. S. (1993) *Methods Enzymol.* **225,** 113–136
10. Olson, G. E., Hamilton, D. W., and Fawcett, D. W. (1976) *Biol. Reprod.* **14,** 517–530
11. Inoue, N., Ikawa, M., Isotani, A., and Okabe, M. (2005) *Nature* **434,** 234–238
12. Carrera, A., Gerton, G. L., and Moss, S. B. (1994) *Dev. Biol.* **165,** 272–284
13. Higgy, N. A., Pastoor, T., Renz, C., Tarnasky, H. A., and Van der Hoorn, F. A. (1994) *Biol. Reprod.* **50,** 1357–1366
14. Vera, J. C., Brito, M., Zuvic, T., and Burzio, L. O. (1984) *J. Biol. Chem.* **259,** 5970–5977
15. Sambrook, J., Fritsch, E., and Maniatis, T. (1989) *Molecular Cloning: A Laboratory Manual,* 2nd Ed., pp. 9.14–9.56, Cold Spring Harbor Laboratory Press, Cold Spring Harbor, NY
16. Russell, L. D., Ettlin, R. A., Sinha, H. A. P., and Clegg, E. D. (1990) *Histological and Histopathological Evaluation of the Testis,* pp. 120–162, Cache River Press, Clearwater, FL
17. Kotaja, N., Kimmins, S., Brancorsini, S., Hentsch, D., Vonesch, J. L., Davidson, I., Parvinen, M., and Sassone-Corsi, P. (2004) *Nat. Methods* **1,** 249–254
18. Tohda, A., Okuno, T., Matsumiya, K., Okabe, M., Kishikawa, H., Dohmae, K., Okuyama, A., and Nishimune, Y. (2002) *Biol. Reprod.* **66,** 85–90
19. Kimura, Y., and Yanagimachi, R. (1995) *Biol. Reprod.* **52,** 709–720
20. Ho, Y., Wigglesworth, K., Eppig, J. J., and Schultz, R. M. (1995) *Mol. Reprod. Dev.* **41,** 232–238
21. Tanaka, H., Miyagawa, Y., Tsujimura, A., Matsumiya, K., Okuyama, A., and Nishimune, Y. (2003) *Mol. Hum. Reprod.* **9,** 69–73
22. Ihara, M., Kinoshita, A., Yamada, S., Tanaka, H., Tanigaki, A., Kitano, A., Goto, M., Okubo, K., Nishiyama, H., Ogawa, O., Takahashi, C., Itohara, S., Nishimune, Y., Noda, M., and Kinoshita, M. (2005). *Dev. Cell* **8,** 343–352
23. Hart, P. E., Glantz, J. N., Orth, J. D., Poynter, G. M., and Salisbury [redacted] (1999) *Genomics* **60,** 111–120
24. Egydio de Carvalho, C., Tanaka, H., Iguchi, N., Ventela, S., Nojima, H., and Nishimune, Y. (2002) *Biol. Reprod.* **66,** 785–795
25. Kyte, J., and Doolittle, R. F. (1982) *J. Mol. Biol.* **157,** 105–132
26. Fawcett, D. W. (1975) *Dev. Biol.* **11,** 391–436
27. Calvin, H. I., and Bedford, J. M. (1971) *J. Reprod. Fertil.* **13,** 65–75
28. Olson, G. E., and Sammons, D. W. (1980) *Biol. Reprod.* **22,** 319–332
29. Cao, W., Gerton, G. L., and Moss, S. B. (2006) *Mol. Cell. Proteomics* **5,** 801–810
30. Miki, K., Qu, W., Goulding, E. H., Willis, W. D., Bunch, D. O., Strader, L. F., Perreault, S. D., Eddy, E. M., and O'Brien, D. A. (2004) *Proc. Natl. Acad. Sci. U. S. A.* **101,** 16501–16506
31. Tanaka, H., Iguchi, N., Isotani, A., Kitamura, K., Toyama, Y., Matsuoka, Y., Onishi, M., Masai, K., Maekawa, M., Toshimori, K., Okabe, M., and Nishimune, Y. (2005) *Mol. Cell. Biol.* **25,** 7107–7119
32. Flickinger, C. J., Baran, M. L., Howards, S. S., and Herr, J. C. (1999) *Anat. Rec.* **254,** 76–86
33. Baillie, A. H. (1962) *J. Anat.* **96,** 335–354
34. Yoshida, K., Kondoh, G., Matsuda, Y., Habu, T., Nishimune, Y., and Morita, T. (1998) *Mol. Cell* **1,** 707–718
35. Bannister, L. A., Pezza, R. J., Donaldson, J. R., de Rooij, D. G., Schimenti, K. J., Camerini-Otero, R. D., and Schimenti, J. C. (2007) *PloS Biol.* 5(5) e
36. De Kretser, D. M., and Baker, H. W. (1999) *J. Clin. Endocrinol. Metab.* [redacted] 3443–3450
37. Tanaka, H., Iguchi, N., Egydio de Carvalho, C., Tadokoro, Y., Yomogida, K., and Nishimune, Y. (2003) *Biol. Reprod.* **69,** 475–482